Bactericidal Effect of Silver Nanoparticles

Determination of size and shape of triangular silver nanoprisms and spherical silver nanoparticles and their bactericidal effect against *Escherichia coli* and *Bacillus subtilis*

Authors

Anders Søbye
Asger Kolding
Jannick Kjær Jørgensen
Marie-Louise Knop Lund
Martin Okkerstrøm Mikkelsen

AALBORG UNIVERSITY
STUDENT REPORT

School of Engineering and Science
Aalborg University 2015
Group 4.212

AALBORG UNIVERSITY
STUDENT REPORT

Third Semester, School of Engineering and Science
Nanotechnology
Skjernvej 4A
9220 Aalborg Ø
http://www.nano.aau.dk

Title:

Bactericidal Effect of Silver Nanoparticles

Project:

P3

Project Period:

September 2014 - January 2015

Projectgroup:

4.212

Participants:

Anders Søbye
Asger Kolding
Jannick K. Jørgensen
Marie-Louise K. Lund
Martin O. Mikkelsen

Supervisors:

Evamaria Petersen
Peter Fojan
Thomas Søndergaard

Printed Copies: 9
Total Page Number: 76
Appendix: 0
Finished: January 5th, 2015

Abstract:

The motivation of this project is to investigate the bactericidal effect of silver nanoparticles (AgNPs). The bactericidal effect of spherical silver nanoparticles (SAgNPs) (0.083 mM and 0.274 mM), triangular silver nanoprisms (TAgNPs) (0.024 mM), and silver ions (0.101 mM and 0.295 mM) are investigated toward the gram-negative bacteria *Escherichia coli* (*E. coli*) and the gram-positive bacteria *Bacillus subtilis* (*B. subtilis*). The bacteria are cultivated in LB broth and YP broth, respectively, and the bactericidal effects of the antimicrobial agents are determined through optical density measurements (OD_{600}). AgNPs are synthesized by a chemical reduction method, and absorption spectroscopy and atomic force microscopy (AFM) are applied to confirm the shape and size of the AgNPs. The antimicrobial agents were suspended into the broths between OD_{600} 0.7 and 1.1. The bactericidal effect of silver ions are well documented, and the silver ions in this project showed a great bactericidal effect. The bactericidal effect of SAgNPs and TAgNPs are also well documented, however, this project revealed no bactericidal effect in the broth experiments. This is suspected to originate in too high concentrations of bacteria in the broth compared to the concentrations of antimicrobial particles.

Preface

This project is written by group 4.212, consisting of third semester Nanotechnology students of Aalborg University from September 3rd to January 5th. Lector Evamaria Petersen, Lector Peter Fojan, and Lector Thomas Søndergaard are the primary supervisors. The topic of the project is nanostructures, which includes nanoparticles and templates. This project will only concern silver nanoparticles as a bactericidal agent.
The project will introduce the topic of nanoparticles and pathogenic bacteria, leading to a problem analysis and problem statement. The statements in the problem analysis and problem limitation are further elaborated throughout the project. Furthermore, the project includes a State of the Art chapter, which concerns with current application of silver nanoparticles in the medical industry. Moreover, the project includes theoretical chapters describing a model of nanoparticles and the antimicrobial effect of silver nanoparticles. A description of the experiment and results will follow, which leads to the end of the project consisting of a discussion and conclusion of the experiment according to relevant theory.
Throughout the project, each chapter and section will have numbered titles. Furthermore, all figures, significant equations, and tables will be numbered. The reference system applied is the numerical system and every reference is then represented by a [number], which refers directly to a specific source in the bibliography. Figures with no reference number are composed by the group itself and vectors are denoted in bold.

Anders Søbye | Asger Kolding | Jannick Kjær Jørgensen

Marie-Louise Knop Lund | Martin Okkerstrøm Mikkelsen

List of Abbreviations

AgNP:	Silver Nanoparticle
SAgNP:	Spherical Silver Nanoparticle
TAgNP:	Triangular Silver Nanoprism
AFM:	Atomic Force Microscopy
SEM:	Scanning Electron Microscopy
TEM:	Transmission Electron Microscopy
PMF:	Proton Motive Force
ROS:	Reactive Oxygen Species
PG:	Peptidoglycan
OD:	Optical Density
LB:	Luria-Bertani
YP:	Yeast Peptone

Table of Contents

1. Introduction

Microorganisms are present all over the earth's biosphere including air, water, and soil, and some microorganisms even thrive under extreme environmental conditions. The human body is a rich habitat for symbiotic microorganisms including bacteria, fungi, and a few protozoa. The human body contains around 600,000 billion cells, where only approximately 60,000 billions of them are human cells. The rest are primarily bacterial cells, which we live in a close vital symbiotic relationship with [1]. However, some microorganisms are pathogenic to the human body, and even our own neutral bacterial flora can become pathogenic in too high concentrations or if they penetrate into the bloodstream or into sterile organs through some surface traumas. [2]

The World Health Organization (WHO) is estimating that pathogens cause around 10 billion infections every year and that 12 million people dies from infectious diseases yearly. Infectious diseases are also among the most common causes of death in humans along with different types of heart and cancer diseases [3]. Most infections caused by pathogenic microorganisms are treatable with antibiotics or other drugs, and some are even preventable by vaccines. However, we face an increase in cases of multi antibiotic resistance in pathogenic microorganisms in the industrial world caused by the heavy use of antibiotics. [3]

Microorganisms are very adaptable to environmental alternations leading to drug resistance in bacteria through development of resistant strains. This induces the need for new alternatives to conventional antibiotics before harmless infections become deadly due to the lack of effective treatments.

The search for new antimicrobial agents opens a new field of nanotechnology, and different approaches are examined today, one include neutral appearing materials as vegetables and herbs, where others include noble metals and even vaginal bacteria [4, 5].

1.1 Problem Analysis

The continuous increase in cases of multi antibiotic and metal ion resistance in pathogenic microorganisms induces the need for constant development of new drugs. However, few new antibiotics have been introduced by the pharmaceutical industry in the last decade, and none have improved activity against multidrug resistance [6, 7]. Furthermore, some antibiotics are proven toxic and allergy inducing in humans, which further motivates the development of new alternative antibiotics that are safe, cost-effective, and with little risk of drug resistance. [7]
One antimicrobial agent that has caught great interest is nanoparticles of noble metals, which have demonstrated great antimicrobial activity making them attractive potential alternatives to antibiotics. Nanoparticles possess unique physiochemical characteristics including extremely high surface-to-volume ratio compared to bulk material, providing a large active surface, high reactivity, and a size ranging in nanometres. [6]
Among the noble metallic nanoparticles, silver nanoparticles have received the greatest attention due to their good conductivity, chemical stability, anti-inflammatory effects, and great antimicrobial activity towards gram-positive and gram-negative bacteria, fungi, and vira [8]. Other noble metal nanoparticles including copper, gold, and titanium nanoparticles have proved some antimicrobial activity, however, silver nanoparticles have proven the most effective antimicrobial agent. Copper is a cheaper alternative to more expensive metal nanoparticles. [7]
It is well known that silver ions and silver based compounds are highly toxic to microorganisms including 16 major species of bacteria [9]. For centuries silver based compounds have been applied in treatment of burn and chronic wounds. However, the use was minimized after the introduction of penicillin in the 1940's [7]. Now silver compounds have once again caught attention and are currently applied in dental works, catheters, and treatment of burn wounds, where they act as antibacterial agents, and control the bacterial growth [10]. The antimicrobial effect of silver compounds is well documented, however, the inhibitory mechanism of silver on microbial growth is only partially known. It is suggested that the antimicrobial effect of silver nanoparticles is a combination of several reactions; penetration of the cell membrane causing structural changes in permeability of the cell membrane, accumulation of nanoparticles on the cell membrane, generation of free radicals leading to a porous cell membrane, deactivation of vital enzymes by reaction between thiol groups and silver ions released from silver nanoparticles, destruction of microbial DNA and RNA, only to mention some of the reactions leading to cell death of pathogenic microorganisms. [9]
When discussing the antimicrobial effect of nanoparticles their size and shape are an important notion. The antimicrobial effect of nanoparticles depends on their small size ranging between 1 and 100 nm, and it is suggested, that a decrease in size will increase antimicrobial activity. Furthermore, the shape of the particle is another leading factor of antimicrobial activity of nanoparticles. It is suggested, that the triangular shape of nanoparticles results in higher antimicrobial activity compared to spherical and rodlike nanoparticles. [8]
Lastly, some precautions must be accounted for when applying silver nanoparticles in antimicrobial treatments including nanotoxicity. There is a need of more profound studies in the field of toxicity of nanoparticles and it is suggested that they are toxic to the

environment, mammalian cells, and cause health problems.
Where metallic silver is inert, silver ions are potentially very reactive. This is important in the antimicrobial action of silver nanoparticles, but can, on the other hand, cause health problems such as Argyria, Argyrosis, and liver and kidney damage. However, there are no regular reports on silver allergy [7, 9]. Furthermore, it is suggested that silver nanoparticles cannot discriminate between different strains of bacteria hence leading to cell death in microbes beneficial to the environment. [9]

1.2 Problem Limitations

This project is limited to the investigation of the bactericidal effect of spherical silver nanoparticles (SAgNPs), triangular silver nanoprisms (TAgNPs), and silver ions toward the gram-negative bacterium *Escherichia coli* (*E. coli*) and the gram-positive bacterium *Bacillus subtilis* (*B. subtilis*) in broths. This project will investigate how the surface-to-volume ratio and the presence of crystallographic facets {111} and {100} affect the bactericidal effect. TAgNPs predominantly have {111} facets where spherical and rod-like, on the other hand, have a high percentage of {100} facets. The {111} facet has the highest atomic density. [8]
Several ways to synthesize silver nanoparticles exist. However, chemical reduction method is by far the most simple to conduct, and it is the easiest one to upscale the production volume of [11]. Chemical reduction method only requires a reduction and stabilizing agent. In this project, SAgNPs are reduced from silver nitrate by sodium borohydride and stabilized by the surfactant polysorbate 80 (Tween 80). TAgNPs are produced, firstly, by reducing silver nitrate by sodium borohydride into nano seeds stabilized by trisodium citrate and, later, silver is reduced by ascorbic acid, stabilized by trisodium citrate, and the growth into nanoprisms is controlled by the surfactant poly(sodium styrene sulphonate).
Both bacteria are grown in broth with environmental conditions optimal for the bacteria. Silver nanoparticles (AgNPs) are added during the exponential growth phase of the bacteria. The antimicrobial effect of the AgNPs are determined by optical density of the culture. A more turbid culture yields a higher absorbance, and is a sign of a higher bacterial concentration. The turbidity of the cultures are determined by absorption spectroscopy measuring the optical density at a wavelength of 600 nm. If the AgNPs have any bactericidal effect toward the bacteria the turbidity of the cultures should decrease as the concentration of metabolic active cells decreases as time progress. The technique is termed turbidimetry.

1.3 Problem Statement

Which of SAgNPs, TAgNPs, and silver ions have the greatest bactericidal effect toward *E. coli* and *B. subtilis*?

2. State of the Art

Various methods have been reported over the last two decades for synthesis of silver nanoparticles (AgNPs), and the majority involves physical and chemical processes. AgNPs can be produced by top-down techniques involving mechanical grinding of bulk metals which are then stabilized by colloidal protecting agents, or bottom-up techniques including chemical reduction methods, electrochemical methods, and sonodecomposition. [9, 12]
Chemical reduction method is by far the most simple one, and it is easy to upscale into large productions. It relies on reduction of metal salts by some chemical reducing agent, and the resulting nanoparticles are 3 - 40 nm in size. The electrochemical method involves electroreduction of silver nitrate in aqueous media containing polyethylene glycol, and produces nanoparticles with a radius of 5 nm. Sonodecomposition involves usage of ultrasonic waves to induce cavitation, which is a phenomenon where ultrasonic waves pass through an aqueous media resulting in microscopic bubbles that expand and eventually burst. The nanoparticles are synthesized by sonochemical reduction of dissolved silver nitrate in an argon-hydrogen atmosphere through generation of hydrogen radicals. The produced nanoparticles are approximately 10 nm in radius. Furthermore, nanoparticles can be synthesized from reduction of silver nitrate by variable frequency microwave radiation resulting in a fast reaction and a high concentration of AgNPs. The produced nanoparticles range from 15 to 25 nm in size. [9]
The main problems with the above mentioned synthesis methods is the use of hazardous chemicals and the extremely expensive nature of the methods. These factors have motivated a search for environmentally friendly biological synthesis methods of metal nanoparticles, which have produced many different, but successful results. Biological synthesis methods involving different leaf extracts and broths have yielded AgNPs with controllable size from 15 to 500 nm [13, 14]. There are, however, still challenges, using this method in relation to shape control and monodispersity. Various microorganisms have also been used to synthesize metal nanoparticles. Klaus *et al.* have reported triangular nanoprisms with differing sizes and a limited control over both size and shape, using the silver resistance in some bacterial cells [15]. Konish *et al.* produced platinum nanoparticles with no mention of size or shape control, using the bacterium *Shewanella Algae* [16]. Enzymes have also been used to synthesise metal nanoparticles along with nanowires [17]. In other experiments, Vigneshwaran *et al.* used a fungus to produce AgNPs, which had a narrow size distribution of 8 ± 1.26 nm. The method used is reported to be very eco-friendly and easy to upscale to large productions. [18]
Kumar *et. al.* show a way of synthesizing SAgNPs in vitro using the enzyme nitrate reductase produce by the fungi *Fusarium oxysporum*. First the fungi is grown, whereupon the nitrate reductase is purified from it. Nitrate reductase is then used to synthesize SAgNPs in vitro under anaerobic conditions and in the presence of α-NADPH and phytochelatin. The SAgNPs should be 9 nm in size. [19]
Another way of producing metal nanoparticles involve green synthesis, where metal nanoparticles are synthesized from leaf extracts. An example of this is described by Geethalaksmi *et al.*. Gold nanoparticles and AgNPs is synthesized from gold (III) chloride

trihydrate and silver nitrate using saponin isolated from aqueous leaf extracts from the plant *Trianthema decandra*. This method produced gold nanoparticles in spherical, hexagonal, and cubic shapes with diameters ranging from 37.7 to 79.9 nm and spherical AgNPs with a diameter ranging from 17.9 to 59.6 nm. [20]
Biosynthesis of AgNPs could also include the use of bacteria as a synthesizing or reducing agent. Shahverdi *et al.* describes a way of synthesizing AgNPs using supernatant from bacteria of the *Enterobacteriacae* family. Supernatant was extracted from bacteria by centrifuging the bacterial culture. Silver nitrate solutions were added to the supernatant, where Ag^{+} was reduced to Ag^{0}. This was succesfully done using the bacteria *E. coli*, *E. cloacae*, and *K. pneumonia*. Compared to methods using bacteria or fungi cell masses, this method is faster, because the reduction of silver occurs more rapidly using the supernatant rather than the bacteria. [21]
A potentially very useful application of the antimicrobial properties of the AgNPs is adsorbing the nanoparticles into different forms of fabrics. Perelshtein *et al.* describes a sonochemical method of adsorbing AgNPs to different forms of fabric where ultrasound is used to fuse the AgNPs with the textile fibres. The treated fabrics, showed great bactericidal effect against both gram-negative (*E. coli*) and gram-positive (*S. aureus*) bacteria. These results show great promise for future use which could include bed linen, wound dressing, and medicinal bandages. These applications could prevent wounds from getting infectious or maybe help treat already existing infections in wounds. [22]
A problem with this approach, is that the antimicrobial agents are always active, which might prolong the healing process of a wound or kill harmless bacteria that are a natural part of the human microflora which might diminish the natural defence against infections. Zhou *et al.* provides a solution to this problem by using vesicles containing the antimicrobial agents instead of applying the antimicrobial agents directly to the wound dressing. Some pathogenic bacteria will secrete toxins that damage the membranes of human cells, thereby killing them. The vesicles are, however, designed to be broken down by the same toxins thus releasing the antimicrobial agents, making the pathogenic bacteria the cause of their own demise. A colorimetric response could also be build into the vesicles thereby giving patients and doctors an early warning of a wound infection. [23]
Just as well as fabrics can be impregnated with AgNPs in order to achieve an antimicrobial effect, so can other surfaces or objects. Implantable medical devices pose a major risk of infections. Once a device has been implanted it gets covered in a biofilm consisting of glycoproteins from tissue and plasma that is insusceptible to most therapeutic agents. Due to this, the device often has to be removed in order to completely eradicate the infection and prevent a relapse. Impregnating these devices with AgNPs shows great potential in the prevention of infections as shown by Furno *et al.*. Silver particles coated onto the surface of the devices have proven ineffective as an antimicrobial agent, most likely, because silver ions are unable to penetrate the biofilm. However, Furno *et el.* have found the AgNPs to be effective when impregnated onto the surface, partially due to a diffusion pressure "pushing" silver ions, released from AgNPs, through the biofilm. [24]

3. Bacterial Microorganisms

Microorganisms include several species such as bacteria, archaea, some fungi and algae, and certain multicellular micro-scaled organisms. Microorganisms are categorized into prokaryotic or eukaryotic cells depending on anatomy and cell structure. Furthermore, prokaryotic cells are divided into the domains of Archaea and Bacteria, while all eukaryotes are placed in one domain of Eukarya. While prokaryotes typically are single cell organisms, eukaryotes can be single or part of a multicellular organism, and are much more complex in structure and composition of intracellular components. [3]
A prokaryotic cell contains several intracellular components, however, none of them are membrane bound. See Figure 3.1 for a three dimensional generalized rodlike bacterium. One other characteristic of prokaryotes is the lack of a true cellular nucleus; in terms of bacteria, their genomes are typically in the form of a single circular strand of DNA (bacterial chromosome), which is an aggregate of hereditary material in the central cell area termed the nucleoid. Some bacteria also contain non-essential (in terms of metabolism) DNA plasmids, which can be transferred between bacteria and often confer the bacteria protective characteristics such as drug resistance and production of toxins and enzymes. Furthermore, bacterial DNA contain only exons, where eukaryotic DNA can contain a large percentage of introns.

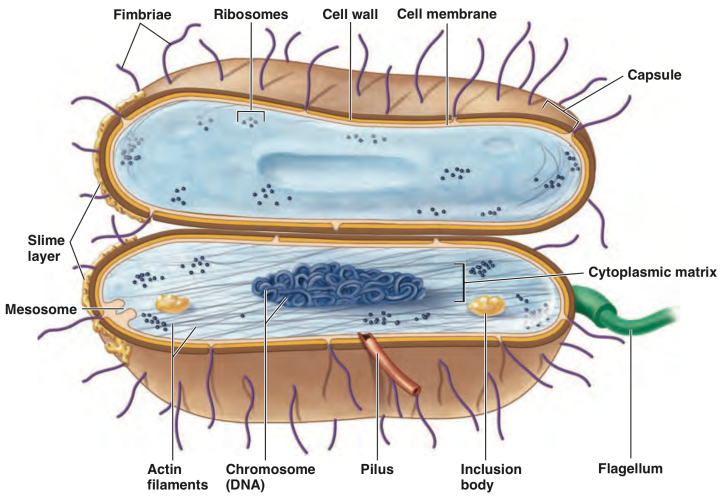

Figure 3.1. A three dimensional illustration of a generalized rodlike bacterial cell structure along with its internal and external components. Notice that this is a generalized model, and not all components are found in all bacterial cells. [3]

On the cell envelope, which encloses the prokaryotic cell, several external components can be found, which often includes mobility appendages such as one or multiple flagella and axial filaments, and attachment or channel appendages such as pilus and fimbriae. These external components are the ones which reacts with the surrounding environments. Like eukaryotes, prokaryotes contain ribosomes, which are the primary protein synthesis site in organisms. [3] The most relevant components and reactions for this project in accordance

with Section 4.5 are further described in this chapter.

3.1 Generalized Model of the Bacterium Envelope

Most bacteria have a chemically complex external envelope surrounding the intracellular components. The cell envelope is composed of two primary layers; the cell wall and the cell membrane. These are often tightly bound together only separated by a thin layer termed the periplasmic space. This space is an important reaction site for substances during transport in and out of the cell. [3]
The cell wall accounts for a number of important bacterial characteristics. In general it helps determine the shape of the bacterium, and it provides an excellent structural support necessary to keep a bacterium from bursting or collapsing due to changes in osmotic pressure. In bacteria, the stability of the cell wall depends on the macromolecule peptidoglycan (PG), which is composed of a repeating framework of long glycan chains, N-acetyl glucosamine and N-acetyl muramic acid alternately, cross-linked by short peptide fragments. The cell wall is crucial to bacterial survival, and if it somehow is missing or incomplete, the bacterium will soon start to lyse. Several types of antimicrobial agents like penicillin target the peptide cross-links, which disrupts the integrity of the PG. [3]
Just beneath the cell wall, the cell membrane exists, which is a thin flexible bilayer of phospholipid units embedded with sulfate and nitrate rich proteins ranging from 5 to 10 nm in thickness. Some membrane proteins are only situated on the surface where other extends through the total membrane. The phospholipids serve as the primary structural component of cell membranes, and are composed of two long apolar fatty acid hydrocarbon chains bound to one glycerol whose third binding site is bound to one phosphate group. The phosphate group is bound to an alcohol group, and the phosphoric acid-alcoholic group is negatively charged resulting in a negatively charged cell membrane, see Figure 3.2.

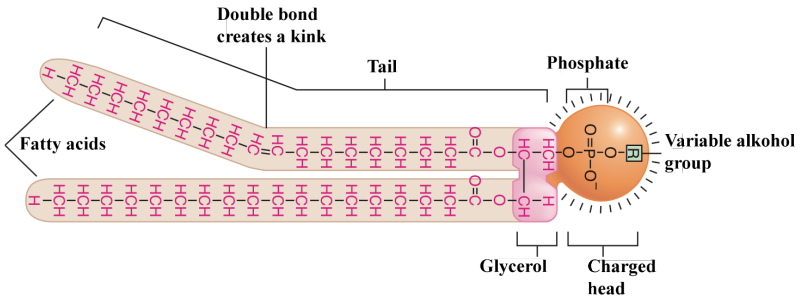

Figure 3.2. Illustration of the general molecular structure of a cell membrane phospholipid. The phospholipids are composed of two long apolar fatty acid hydrocarbon chains bound to one glycerol whose third binding site is bound to one phosphate group. The phosphate group is bound to an alcohol group, and the phosphoric acid-alcoholic group is negatively charged resulting in a negativly charged cell membrane. [3]

Bacterial cell membranes generally consist of 30 - 40 % phospholipids and 60 - 70 % proteins of the total membrane mass. Prokaryotes that differ significantly from this model are mycoplasma- and archaea membranes. [3]

The lipid phase is in motion and thus the cell membrane is dynamic, constantly changing, and proteins migrate freely around. The major role of regulating transport by selective permeable proteins is primarily completed by the cell membrane although the cell wall can bar the passage of larger molecules. In bacteria, the membrane provides an important site for energy reactions, nutrient processing, and synthesis. Most enzymes essential for energy reactions of respiration in bacteria resides in the cell membrane. [3]
The cell envelope can include one or two cytoplasmic lipid membranes classifying the bacterium as either gram-positive or gram-negative. The gram-positive bacteria envelope contains one thick PG cell wall ranging from 20 to 80 nm in thickness and one cell membrane. Moreover, the cell wall is composed of tightly bound acidic polysaccharides, which include teichoic- and lipoteichoic acid, where teichoic acid is a polymer of ribitol or glycerol and phosphate that is embedded into the framework of PG, and lipoteichoic is similarly a polymer, but is instead attached to lipids in the cell membrane. The gram-positive bacteria either have a very thin, or no periplasmic space. [3]
On the other hand, the gram-negative bacteria, besides a thinner single PG layer ranging 1 - 3 nm and a cell membrane, contains one outer membrane making it more complex in morphology. This membrane is similar in construction to the cell membrane; except the fact that it contains specialized types of lipopolysaccharides (LPs) and lipoproteins. LPs are composed of lipid molecules bound to polysaccharides. The lipid molecules make up the top layer matrix of the membrane. Located in the top layer one will find porins that act as transport proteins regulating molecules during transport in and out of the cell, and on the bottom layer one will mainly find phospholipids and lipoproteins. The selective permeability of gram-negative bacteria relies on the porin proteins. The thin PG layer assigns the gram-negative bacteria greater flexibility and sensitivity to lysis. Surrounding the PG layer, one will find two extensive periplasmic spaces. [3]
The envelope structure of a gram-positive and a gram-negative bacterium is illustrated in Figure 3.3.

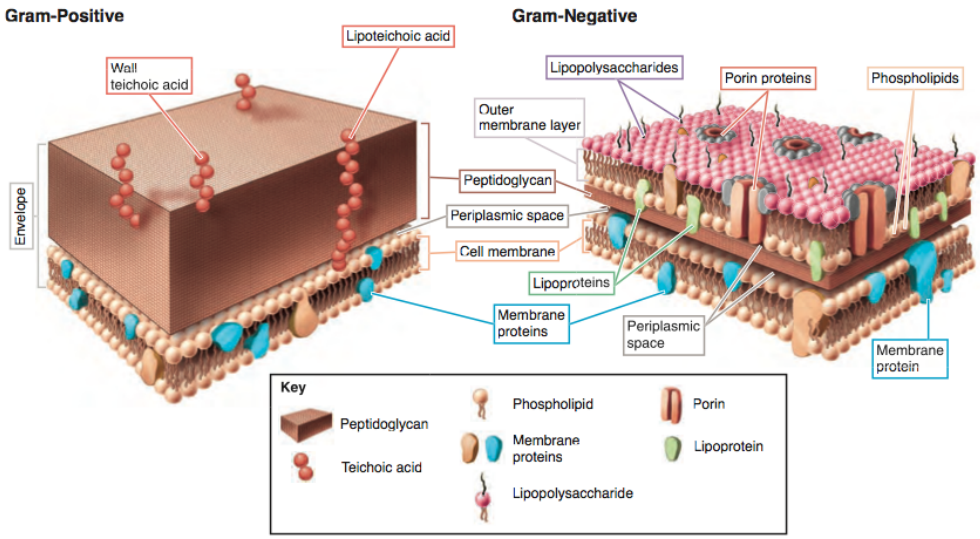

Figure 3.3. A three-dimensional illustration of the gram-negative and gram-positive cell envelope. In the case of the gram-positive cell envelope, a thick (20 - 80 nm) cell wall and a cell membrane are present. In the case of the gram-negative cell envelope, a thin (1 - 3 nm) cell wall, a cell membrane, and an outer cell membrane are present. [3]

Due to the extra membrane layer, the gram-negative bacterium is more impervious to some antimicrobial chemicals making them more difficult to inhibit or kill. One exception is alcohol-based compounds that can potentially dissolve the lipids in the outer membrane disturbing its integrity. Several bacterial groups lack the cell wall structure of gram-negative and gram-positive, and some do not have a cell wall at all (Mycoplasmas). Mycoplasmas resist bursting and collapsing by sterols incorporated into the cell membrane. [3]

3.2 Intracellular Components

The intracellular components of the bacterial cell reside in a complex solution termed the cytoplasm, or cytoplasmic matrix. This solution serves as a site for biochemical and synthetic cell activities. Its primary component is water ranging from 70 to 80 %, which serves as solvent for a mixture of nutrients including sugars, amino acids, and other organic molecules and salts, which provides necessary building blocks for cell synthesis or as energy sources. Furthermore, the cytoplasm contains larger, discrete components such as the bacterium chromosome, ribosomes, granules, and actin strands. The composition of the intracellular components vary within bacterium species. [3]
A bacterial cell typically contains a large number of ribosomes, that are chemically composed of about 60 % rRNA and about 40 % protein. The ribosomes are the primary protein synthesis site of all living cells, and they differ in size, composition ratio, and structure between bacteria and eukarya, making them a potential antimicrobial action site. Some antimicrobial agents inhibit bacterial ribosomes while eukarya ribosomes remain unharmed. [3] Lastly it is proposed that certain bacterial species possess an intracellular network of protein polymers (actin strands), which, along with the cell wall, contribute to cell stability and integrity. Chemically, the proteins are similar to actin filaments of the eukaryotic cytoskeleton, and are therefore termed bacterial actin. [3]

3.3 Bacterial Cell Growth

Microorganisms that are provided with nutrients and the required environmental factors are metabolically active, and growing in terms of population, and synthesis of cellular components resulting in an increase in size [3]. This section is based upon characteristics of bacterial growth in single-celled microorganisms.
In bacteria, cell division primarily occurs through binary transverse fission, where one parent cell becomes two daughter cells in the transverse plane. During binary fission, the parent cell increases its size, duplicates its chromosome, and forms a central transverse septum that finally divides the parent cell into two daughter cells. This cycle is a continuous process in bacterial colonies resulting in an increase in bacterial population, and the duration of it is termed the generation time. [3]
Compared to other organisms, bacteria grow with a rapid rate; the average generation time is between 30 and 60 minutes under optimum conditions. However, they will not continue doubling at a maximum rate. Eventually several biotic and abiotic factors will prevent cell division leading to cell death and a decrease in population. In systems of finite space and nutrients with no waste removal mechanisms the bacterial lifespan is described over 3 to 4 days in a growth curve. The curve consists of a series of phases; the lag phase, the

exponential growth phase, the stationary phase, and the death phase. [3]
In the lag phase, the bacterial population is not increasing. The individual cells are adjusting to the environment and are metabolically active resulting in an increase in size and a synthesis of chromosomes, enzymes, and ribosomes. The length of the lag phase varies between populations depending on the bacteria and growth media. [3]
In the exponential (logarithmic or log) growth phase, the bacterial population reaches its minimum generation time, and at the end, its maximum population number. This phase will continue until nutrients are no longer adequate for exponential growth. Microorganisms in this active phase are more vulnerable to antimicrobial agents that disrupt cell metabolism and binary fission compared to those in the next phase. [3]
In the stationary phase the bacterial population has reached its maximum. The curve appears stationary since the rate of cell death balances out the rate of cell multiplication. Normally at this state, the level of nutrients and oxygen becomes limited, leading to cell death, along with the high level of organic acids and other toxic biochemicals from the high density of bacterial cells. Eventually the cells become unable to multiply due to the lack of nutrients, and all bacteria begin to lyse, resulting in the last growth phase; the death phase. The death rate in this phase is exponential, and the speed of decay depends on the relative resistance of the species and the level of toxins in the media. However, the rate is usually slower than the rate of the exponential growth phase [3]. See Figure 3.4 for a full, generalized growth curve.

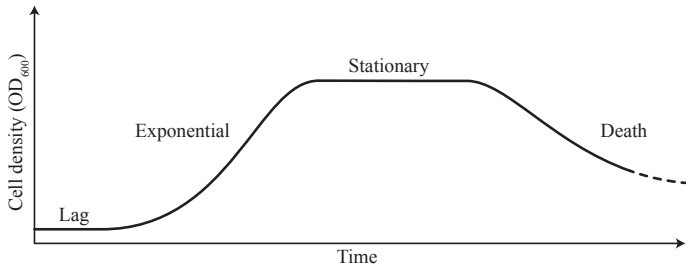

Figure 3.4. Generalized bacterial growth curve illustrating the lag phase, exponential phase, stationary phase, and the death phase. The death phase depends on the individual bacterium species.

Although bacteria are very adaptable to adverse habitats, nothing can be compared to bacterial endospores. Endospores are dormant bodies produced by bacteria, including *Bacillus*, and are a part of the two-phased life cycle of these bacteria, shifting between vegetative cells and endospores. The vegetative cell is the metabolic active one, and when exposed to certain environmental signals forms an endospore by sporulation. The spore is inert, highly resistant to almost everything, and fitted for long-term survival. [3]

3.3.1 Cultivation of Microorganisms

To cultivate microorganisms, one will need a container of nutrient medium, which provides an environment suitable for the cultivated microorganism to grow in. The medium needs to provide carbon, nitrogen, energy sources, and vitamins and trace minerals as well as a growth base with minimal or no cellular adaptation, and demonstrate ability to maintain cell population for an extended period of time. [25]
Growth media are categorized by their physical state, chemical composition, and functional

type. Media described here are designed for bacteria and fungi growth, and will only concern liquid and solid media.
Liquid media are fabricated by dissolving media components in distilled water and are thus defined as water-based solutions that do not solidify at temperatures above freezing. These media are termed broths, milks, or infusions, and bacterial growth occurs throughout the media by a dispersed, cloudy, or flaky appearance. [3]
Likewise, solid media are fabricated by dissolving media components in distilled water. However, solid media additionally contain solidifying agents, most often agar, which changes the physical properties of the medium in response to temperature. Once liquefied at 100 °C, agar re-solidifies around 42 °C, and provides a firm, hard surface on which cells can form discrete colonies. Agar is a complex polymer of galactose and sulphur-containing carbohydrates that provides a basic framework to hold nutrients and moisture in the medium. [3]
The nutritional and environmental requirements of bacterial species is specific, indicating that the growth media must obey these requirements for the cells to grow optimally. The media composition is either chemically defined (synthetic media) or complex, meaning that either all components of the media is expressed by chemical formulas, or one or few components of the media are indefinable. Indefinable components often refer to extracts from animal or plant tissue or blood, milk, or digests like peptone or tryptone. The benefits of complex media are that they are often inexpensive, and they support growth of a large variety of microorganisms. [3]
Peptone and tryptone are partially digested proteins, rich in amino acids, that are often used as primary carbon and nitrogen sources in a growth medium. Peptone is proteins, either partially enzymatic digested or partially acid hydrolysed into a protein intermediate. Peptones are preferably partially digested into peptides compared to being fully digested into amino acids, since several bacteria prefer peptides to amino acids. Tryptone is a peptone digest of casein protein originated from milk. Both peptone and tryptone are water-soluble and both provide an excellent carbon source as well as a nitrogen source. However, they generally provide different amounts of specific amino acids due to the origin of the proteins. The origin of the peptone protein must be specified if it is to be applied. [3, 25]
Furthermore, it is necessary to provide the medium with vitamins. One inexpensive source is yeast extract that not only provides vitamins, but also proteins, carbohydrates, and other micronutrients. Yeast extract is a water-soluble, peptone-like derivative of yeast cells. [25]
Lastly, most organisms require an isotonic or hypotonic environment for optimal growth, and particularly sodium chloride to maintain osmolality. In these environments, water either flows in and out of the cell at equal rates (isotonic), or only into the cell (hypotonic). Furthermore, most bacteria require salts such as magnesium, calcium, iron, and potassium salts for bacterial growth as they provide elements used for cofactors in certain enzymatic reactions. [26]

3.3.2 Turbidimetry

One of the simplest existing techniques of estimating the size of a bacterial population is by turbidimetry [3]. Turbidimetry is the measurement of the cloudiness or turbidness of a culture broth, that gradually becomes more turbid with increasing concentration of

bacterial cells starting in clear broth. The turbidity can be measured by means of a light sensitive instrument like a spectrophotometer. The spectrophotometer is equipped with a light source that sends monochromatic light through a sample cuvette, and a photodetector that measures the light intensity through the sample. As the cell population increases, the light intensity through the sample decreases, resulting in higher absorbance. Less light will reach the photodetector and more will be absorbed or scattered by the cells themselves. When entering the cuvette, the incident light will be subjected to three interactions; some will be absorbed by the cells, some will be transmitted through the sample, and some will be scattered by the cells. When measuring OD using light with a wavelength between 400 and 1000 nm, bacterial cells primarily scatter the incident light. The absorbance of light at these wavelengths by the bacterial cells is weak compared to when using UV light. The scattering originates from the different refractive index inside the bacteria, compared to the media, which is typically 1.39. This is enough to scatter the incident light. [27] The standard light used for turbidimetry is monochromatic visible light at a wavelength of 600 nm, thus the optical density (OD) is OD_{600} [3].
However, some problems must be accounted for when using turbidimetry. For example, the spectrophotometer cannot differentiate between metabolic active and dead cells resulting in an OD representing total cell density. Furthermore, microscopic air bubbles are measured as metabolic active cells, and in dense populations, the concentration of air bubbles might be quite high.
When the OD_{600} exceeds 0.7, there is a deviation from the Lambert-Beer law, resulting in a poor estimation of cell density. The Lambert-Beer law relates the light intensity with the length of the optical path and the concentration of the absorbing and scattering particles [28]. The law, however, is only valid at low concentrations of the particles, and when the OD_{600} value exceed 0.7, the culture broth must be diluted before measurement [29].

3.4 *Escherichia coli*

Escherichia coli (*E. coli*), see Figure 3.5, is a gram-negative, rodlike facultative anaerobe bacterium, that ferments lactose but prefers aerobic respiration when oxygen is present. The *E. coli* chromosome contains 4,288 genes and measures about 1 mm if unfolded linearly. In comparison, the bacterium is only 1 µm in length. The normal generation time is approximately 20 minutes, making it an ideal, and traditional, cloning host. [3]

Figure 3.5. The rodlike *Escherichia coli* bacterium [30].

A common habitat of *E. coli* is the digestive tract of most warm-blooded animals where it lives symbiotically with the host, producing vitamins and acids beneficial to the host,

and produces proteins toxic to other intestine pathogens. However, in large concentrations *E. coli* becomes pathogenic; it is a major cause of food and water poisoning resulting in diarrhoea. Furthermore, 80 % of urinary tract infections can be traced to *E. coli*. Different strains and serotypes of *E. coli* posses different pathogenic characteristics. However, it is not classified as a true pathogenic. [3].
E. coli is best cultivated at a temperature of 37 °C, and according to ATCC, it is best cultivated in Luria-Bertani (LB) medium, which is an all-purpose medium consisting of tryptone, yeast extract and sodium chloride, either as broth or with agar. [26]

3.5 *Bacillus subtilis*

Bacillus Subtilis (*B. subtilis*), see Figure 3.6, is a gram-positive, rodlike facultative anaerobe bacterium, once thought to be an obligate aerobe, that grows by anaerobic respiration when nitrate is present, or fermentation when glucose and pyruvate are present [31]. The *B. subtilis* chromosome contains approximately 4,100 genes [32] and the bacterium measures 1 - 5 µm in length [32]. Under optimal growth conditions, the generation time of *B. subtilis* varies between 26 and 45 minutes, but is observed as high as 120 minutes. Its natural habitat includes soil, water, air, and decomposing plant material. Furthermore, *B. subtilis* is capable of producing endospores when the environment is unfavourable for the bacterium. [3, 25]
B. subtilis is used in production of antimicrobial agents, because it produces a class of lipopeptide antibiotics including iturins, which favour the survival of *B. subtilis* by outcompeting other microorganisms like bacteria and fungi. *B. subtilis* bacteria are not true human pathogens, and are rarely isolated from infections in humans. [3, 26]
Like most environmental strains, *B. subtilis* is optimally cultivated at temperatures between 25 and 30 °C [26], however, it is also observed to be 30 to 37 °C, with minimum growth temperature 18 °C and maximum 43 °C [33]. *B. subtilis* is capable of adapting to changes in osmotic pressure and saline conditions, but it is observed to grow most optimally in media with no or very little salt concentration. [34]

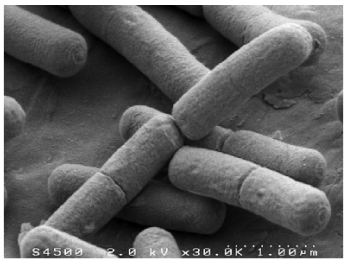

Figure 3.6. SEM picture of the rodlike *Bacillus subtilis* bacterium. [35]

4. Silver Nanoparticles

Nanotechnology literally means any technology on the nanometer scale. Following that, a nanoparticle is defined as an aggregate of atoms bonded together with a radius ranging from 1 to 100 nm, typically consisting of 10 to 10^5 atoms. Nanoparticles often have extraordinary properties compared to bulk sized particles including optical, magnetic, electronic, and catalytic properties, due to quantum mechanical effects, which only occur on the nanometer scale. An example of this is gold, which in bulk size is a noble metal that usually is inert. However, gold nanoparticles with a size of 2 - 3 nm are quite reactive and can cause chemical reactions to occur faster than they would if bigger particles were used. This is a consequence of the fact that chemical reactions occur on the surface of particles and as the particle-size decreases, the surface-to-volume ratio increases. A cube consisting of one billion atoms has a side length of roughly 300 nm and 0.6 % of the atoms will be on the surface of the cube. Another cube with a side length of 3 nm on every side consists of a thousand atoms and 50 % will be on the surface of the particle. [36, 37]
Like gold, silver nanoparticles (AgNPs) are also much more reactive than bulk silver due to the higher surface-to-volume ratio. Due to the great reactivity of nanoparticles, they have caught great attention in treatment of infectious diseases where they act as antimicrobial agents.
The silver atoms aggregate into nanoparticles in an ordered manner. The most common crystal structure of silver is the face-centered cubic system, which include crystallographic facets as {111}, {100} and {110} dependent on axis contact of the facet [38], see Figure 4.1. The surface composition confers the particle unique colloidal properties, where larger surface-to-volume ratio supposedly results in a larger antimicrobial effect. Different morphologies can result from changing the relative growth rates of different crystallographic facets by surface-modifying or capping agents, but also parameters such as time and temperature can affect the morphology of the particle. In antimicrobial context, two interesting morphologies of AgNPs are the spherical silver nanoparticle (SAgNP) and the triangular silver nanoprism (TAgNP). [39]

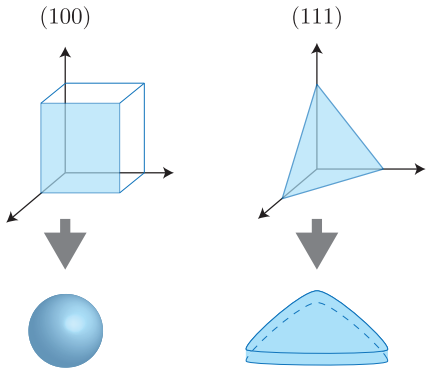

Figure 4.1. Illustration of two important crystallographic facets of the face-centered cubic system. The {111} facets are predominantly present in TAgNPs, where the {100} facets are predominantly present in SAgNPs.

To determine the morphologies of nanoparticles, one can measure light absorption on the particles using a spectrophotometer when exposed to different incident light wavelengths. The result is an absorption spectra specific for the particle morphology with a maximum absorption wavelength defined by the particle acting as an oscillating dipole. One can predict the absorption spectra of a specific nanoparticle by the behaviour of the particle exposed to electromagnetic waves. The absorption cross-section is a measurement of the probability of particle and light interaction.

4.1 Absorption of Spherical Silver Nanoparticles

When exposed to light, a SAgNP with a significantly small diameter compared to the wavelength of the visible light experiences an increased interaction with the electromagnetic wave compared to those with a larger diameter. This effect can be described by making some assumptions about the nanoparticle; the particle must be extremely small compared to the wavelength of the electromagnetic wave and when suspended, the particles are far away from each other.

From the first assumption, one can assume that the electromagnetic field of the electromagnetic wave is homogeneous around the nanoparticle. The contribution of the magnetic field of the electromagnetic wave to the interaction is significantly small, and therefore only the electric field (E-field) is accounted for, see Figure 4.2. In the external E-field, the free electrons of the nanoparticle are slightly displaced in relation to the nanoparticle creating a partially negative and positive side on the particle. This creates an induced internal E-field inside the nanoparticle. The particle is polarized by the external E-field, and is essentially an electric dipole. As time progress, the dipole oscillates, following the electromagnetic wave oscillation. As the external E-field induces the dipole, some of the light will be absorbed in the nanoparticle with a maximum amount of absorption at a specific frequency, termed the plasmon resonance frequency [40]. The plasmon resonance frequency is directly related to a specific wavelength of the incident electromagnetic wave, and can be visualized with absorption spectroscopy [41, 42].

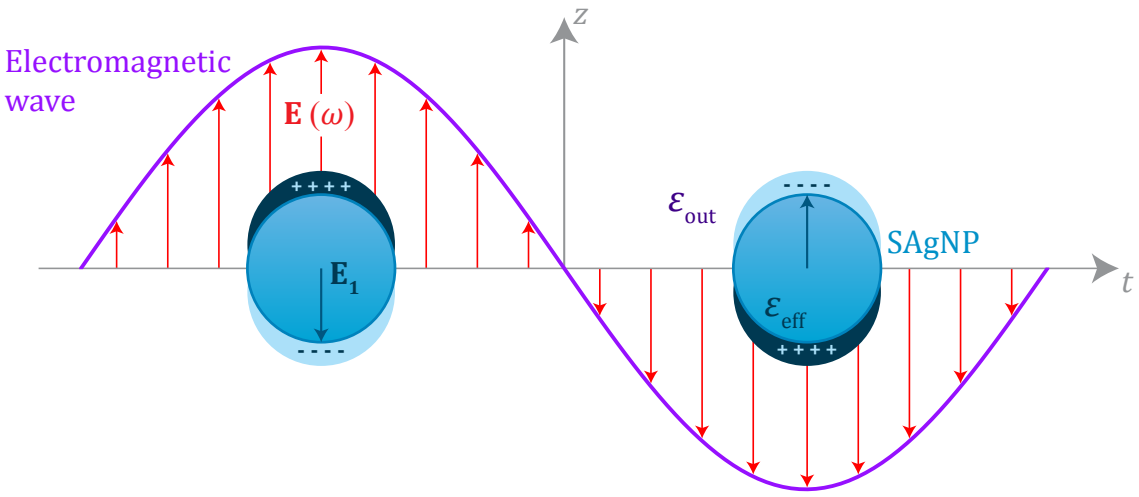

Figure 4.2. Illustration of a nanoparticle exposed to an external E-field ($\mathbf{E}(\omega)$) from an incident electromagnetic wave resulting in the nanoparticle acting as an oscillating dipole in the z-direction, creating an internal oscillating E-field ($\mathbf{E_1}$).

When the light wave interacts with the nanoparticle some of the light will be absorbed in the nanoparticle, and some will be scattered throughout the medium. However, the scattered part is considered negligible in comparison to the absorption. To describe this phenomenon, the absorption cross-section is introduced. The absorption cross-section is related to the probability, and amount of absorption interactions in a sample at specific wavelengths. The maximum absorption wavelength ($\lambda_{\max}$) is equal to the maximum absorption cross-section wavelength. The absorption cross-section is defined in Equation (4.1).

$$\sigma_{\text{abs}} = \frac{P_{\text{abs}}}{I_0}, \tag{4.1}$$

where P_{abs} is the effect of the absorbed light and I_0 is the intensity of the incident light.

4.1.1 Dielectric Constant of a Metal Nanoparticle

In order to determine the effect of the absorbed light, one will need to introduce the dielectric constant of the nanoparticle. The dielectric constant varies with the wavelength of the incident light. To determine the dielectric constant, the current density is introduced, which is described by the movement of the electrons in the particle. Following Drudes theory of free electrons, the electrons inside the nanoparticle are considered to be free and independent of each other. Thus when the electrons are moved as a unit their movement can be considered as the sum of the motion of the individual electrons. The motion of one electron can be found by equation (4.2), which describes the force acting on the electron. [42]

$$m_{\text{e}} \cdot \frac{d\mathbf{v}}{dt} + m_{\text{e}}\Gamma\mathbf{v} = e\mathbf{E}, \tag{4.2}$$

where m_{e} is the effective electron mass, e is the charge of the electron, $\mathbf{v}$ is the electron velocity, and Γ is a dampening constant [42]. As the light wave propagates sinusoidal by $\mathbf{E}(\omega) = \mathbf{E_0} \cdot e^{-i\omega t}$, the electron velocity also propagates sinusoidally as it changes with the external E-field, $\mathbf{v} = \mathbf{v_0} \cdot e^{-i\omega t}$. Compiled into Equation (4.2), one will find Equation (4.3),

$$(-i\omega m_{\text{e}} + m_{\text{e}}\Gamma)\mathbf{v_0} \cdot e^{-i\omega t} = e \cdot \mathbf{E_0} \cdot e^{-i\omega t}. \tag{4.3}$$

Isolating $\mathbf{v_0}$ from Equation (4.3), it can be written that

$$\mathbf{v_0} = \frac{e}{m_{\text{e}}\Gamma - i\omega m_{\text{e}}}\mathbf{E_0}. \tag{4.4}$$

The current density is defined by the individual motion of the electrons times the electron density n and the electron charge,

$$\mathbf{J} = e \cdot n \cdot \mathbf{v_0} = \frac{n \cdot e^2}{m_{\text{e}}\Gamma - i\omega m_{\text{e}}}\mathbf{E_0}. \tag{4.5}$$

Furthermore, the current density can be defined as the particle conductivity $\sigma(\omega)$ times the vector amplitude of the external E-field $\mathbf{E_0}$. Conclusively, the fraction on the right-hand side of Equation (4.5) must be equal to the particle conductivity:

$$\sigma(\omega) = \frac{n \cdot e^2}{m_{\text{e}}\Gamma - i\omega m_{\text{e}}}. \tag{4.6}$$

Equation (4.6) yields that the particle conductivity is dependent on the frequency of the light and thus on the light wavelength. Note that the particle conductivity is complex.

Furthermore, the current density $\mathbf{J}$ is described as the change over time in polarisation $\mathbf{P}$ of the AgNP by the external E-field $\mathbf{J} = \frac{\partial \mathbf{P}}{\partial t}$, where $\mathbf{P}$ being $\mathbf{P} = \mathbf{P_0} \cdot e^{-i\omega t}$. Thus

$$\mathbf{J} = -i\omega \cdot \mathbf{P} \Rightarrow \mathbf{P} = -\frac{1}{i\omega}\mathbf{J} = \frac{i}{\omega} \cdot \sigma(\omega) \cdot \mathbf{E_0}. \tag{4.7}$$

The displacement field induced by the external E-field in the particle is defined and combined with Equation (4.5), yielding

$$\mathbf{D} = \varepsilon_0 \cdot \varepsilon_\mathrm{r} \cdot \mathbf{E_0} = \varepsilon_0 \cdot \mathbf{E_0} + \mathbf{P} = \left(\varepsilon_0 + \frac{i}{\omega}\sigma(\omega)\right) \cdot \mathbf{E_0} = \varepsilon_0 \cdot \left(1 + \frac{i}{\omega\varepsilon_0}\sigma(\omega)\right) \cdot \mathbf{E_0}.$$

The last parenthesis is known as the complex dielectric constant or effective dielectric constant ε_eff of the nanoparticle.
Inserting the particle conductivity from equation (4.6) into the parenthesis yields

$$\varepsilon_\mathrm{eff} = 1 + \frac{i}{\omega\varepsilon_0} \cdot \frac{ne^2}{m_\mathrm{e}\Gamma - i\omega m_\mathrm{e}} = 1 + \frac{i\omega_\mathrm{p}^2}{\omega(\Gamma - i\omega)} = 1 - \frac{\omega_\mathrm{p}^2}{\omega(\omega + i\Gamma)}. \tag{4.8}$$

Here $\omega_\mathrm{p}^2 = \frac{ne^2}{\varepsilon_0 m_\mathrm{e}}$. For later it is important to note that $\Re(\sigma(\omega)) = \omega\varepsilon_0 \cdot \Im(\varepsilon_\mathrm{eff})$. The internal E-field of the nanoparticle is nextly determined in order to find the effect of the absorbed light.

4.1.2 Internal Electric Field of the Nanoparticle

The electric field $\mathbf{E}(\omega)$ around a spherical nanoparticle, with radius r_s and dielectric constant ε_eff in a medium that has dielectric constant ε_out, is homogeneous and points in the z-direction in this model. The electrostatic potential inside and outside the nanoparticle is introduced, where, using spherical zonal harmonics derived from Legendre's polynomials, the solution is guessed to be satisfied by a sum of the two lowest order zonal harmonics. [43]
Inside the nanoparticle

$$\phi_1(r, \theta) = A_1 \cdot r \cdot cos(\theta) + C_1 \cdot r^{-2} \cdot cos(\theta). \tag{4.9}$$

Outside the nanoparticle

$$\phi_2(r, \theta) = A_2 \cdot r \cdot cos(\theta) + C_2 \cdot r^{-2} \cdot cos(\theta). \tag{4.10}$$

Far away from the particle, the external E-field is uniform and there is no contribution from the nanoparticle. The electrostatic potential becomes, as if no particles were present at all, $-E_0 \cdot r \cdot cos(\theta)$. Thus $A_2 = -E_0$. C_1 must be zero, as otherwise the external E-field and potential would become infinite at the center of the spherical nanoparticle. Lastly, the constants A_1 and C_2 can be determined through boundary conditions, at the surface of the nanoparticle, as $\phi_1 = \phi_2$ at $r = r_s$. [43] Consequently

$$-E_0 \cdot r_\mathrm{s} \cdot \cos\theta + C_2 \cdot r_\mathrm{s}^{-2} \cdot \cos\theta = A_1 \cdot r_\mathrm{s} \cdot \cos\theta. \tag{4.11}$$

The boundary conditions for the external E-field is expressed through the radial part of the displacement field $D_\mathrm{out}^\perp - D_\mathrm{in}^\perp = \sigma_\mathrm{free}$. However, the surface charge is $\sigma_\mathrm{free} = 0$, and

$D_{\text{out}}^{\perp} = D_{\text{in}}^{\perp}$. Moreover, the radial part of the displacement field is expressed by the change in electrostatic potential $D^{\perp} = -\varepsilon\left(\frac{\partial\phi}{\partial r}\right)$. Thus

$$\varepsilon_{\text{out}} \cdot \left(E_0 \cdot \cos\theta + 2C_2 \cdot r_{\text{s}}^{-3} \cdot \cos\theta\right) = -\varepsilon_{\text{eff}} \cdot A_1 \cdot \cos\theta. \tag{4.12}$$

Equations (4.11) and (4.12) are two equations with two unkown quantities. Cosine can be discarded, and C_2 does not need to be isolated as only the internal potential is of relevance. Equations (4.11) and (4.12) are combined to express A_1 as

$$A_1 = -\frac{3 \cdot E_0 \cdot \varepsilon_{\text{out}}}{\varepsilon_{\text{eff}} + 2 \cdot \varepsilon_{\text{out}}}.$$

Thus the potential inside the nanoparticle is

$$\phi_1(r,\theta) = -\frac{3 \cdot E_0 \cdot \varepsilon_{\text{out}}}{\varepsilon_{\text{eff}} + 2 \cdot \varepsilon_{\text{out}}} \cdot r \cdot \cos\theta. \tag{4.13}$$

Only the E-field inside the nanoparticle is important as this field is the one used to find the effect, and later the absorption cross-section. It is defined as $\mathbf{E} = -\nabla\phi$, and

$$\mathbf{E_1} = \frac{3\varepsilon_{\text{out}}}{\varepsilon_{\text{eff}} + 2\varepsilon_{\text{out}}} \cdot \mathbf{E_0}. \tag{4.14}$$

From Equation (4.14), it is evident that the internal E-field is at maximum when $\varepsilon_{\text{eff}} \to -2\varepsilon_{\text{out}}$.

4.1.3 Effect of Absorbed Light

Remember that the absorption cross section is defined by the effect of the absorbed light. The effect is defined by

$$P_{\text{abs}} = \left\langle \int_{\mathcal{V}} \mathbf{J} \cdot \mathbf{E}(\omega)\ \mathrm{d}\tau \right\rangle.$$

The external E-field $\mathbf{E}(\omega)$ is only defined by the real part of the internal E-field $\mathbf{E_1}$. $\mathbf{E}(\omega) = \Re\left(\tilde{\mathbf{E_1}} \cdot e^{-i\omega t}\right) = \frac{1}{2}\left(\tilde{\mathbf{E_1}} \cdot e^{-i\omega t}\right) + \frac{1}{2}\left(\tilde{\mathbf{E_1^*}} \cdot e^{i\omega t}\right)$. The same is true for the current density. Thus

$$P_{abs} = \left\langle \int_{\mathcal{V}} \frac{1}{2}\left(\tilde{\mathbf{J_1}} \cdot e^{-i\omega t} + \tilde{\mathbf{J_1^*}} \cdot e^{i\omega t}\right) \cdot \frac{1}{2}\left(\tilde{\mathbf{E_1}} \cdot e^{-i\omega t} + \tilde{\mathbf{E_1^*}} \cdot e^{i\omega t}\right)\ \mathrm{d}\tau \right\rangle.$$

$$\Downarrow$$

$$P_{\text{abs}} = \left\langle \int_{\mathcal{V}} \frac{1}{4}\left(\left(\tilde{\mathbf{J_1}} \cdot \tilde{\mathbf{E_1^*}}\right) + \left(\tilde{\mathbf{J_1^*}} \cdot \tilde{\mathbf{E_1}}\right) + \left(\tilde{\mathbf{J_1}} \cdot \tilde{\mathbf{E_1}}\right) e^{-2i\omega t} + \left(\tilde{\mathbf{J_1^*}} \cdot \tilde{\mathbf{E_1^*}}\right) e^{2i\omega t}\right) \mathrm{d}\tau \right\rangle.$$

The effect is averaged over time. As $\left\langle e^{-2i\omega t}\right\rangle = \left\langle e^{2i\omega t}\right\rangle = 0$, and as the integral does not depend on the current density nor the E-field, it yields

$$P_{\text{abs}} = \frac{V}{4}\left(\left(\tilde{\mathbf{J_1}} \cdot \tilde{\mathbf{E_1^*}}\right) + \left(\tilde{\mathbf{J_1^*}} \cdot \tilde{\mathbf{E_1}}\right)\right).$$

As both current density and the internal E-field is present with their complex conjugate, it can be shortened as the real part of the product

$$P_{\text{abs}} = \frac{V}{2} \cdot \Re(\tilde{\mathbf{J_1}} \cdot \tilde{\mathbf{E_1^*}}).$$

As $\tilde{\mathbf{J_1}} = \sigma(\omega) \cdot \tilde{\mathbf{E_1}}$, the equation becomes

$$P_{\text{abs}} = \frac{V}{2}\Re\left(\sigma(\omega) \cdot \tilde{\mathbf{E_1}} \cdot \tilde{\mathbf{E_1}}^*\right) = \frac{V}{2}\Re\left(\sigma(\omega) \cdot |\tilde{\mathbf{E_1}}|^2\right).$$

Inserting Equation (4.5) for the particle conductivity $\sigma(\omega)$ and Equation (4.14) for the internal E-field $\mathbf{E_1}$, it can be written that

$$P_{\text{abs}} = \frac{V}{2}\left(\omega\varepsilon_0 \cdot \Im(\varepsilon_{\text{eff}}) \cdot \left|\frac{3\varepsilon_{\text{out}}}{\varepsilon_{\text{eff}} + 2\varepsilon_{\text{out}}} \cdot \mathbf{E_0}\right|^2\right).$$

$$\Downarrow$$

$$P_{\text{abs}} = \frac{V}{2}\left(\omega\varepsilon_0 \cdot \Im(\varepsilon_{\text{eff}}) \cdot \frac{9 \cdot \varepsilon_{\text{out}}^2}{|\varepsilon_{\text{eff}} + 2\varepsilon_{out}|^2} \cdot |\mathbf{E_0}|^2\right). \tag{4.15}$$

Now, one will only need to determine the intensity of the incident electromagnetic wave to express the absorption cross-section.

4.1.4 Intensity of Incident Light

The poynting vector is pointing in the propagation direction of the electromagnetic wave. The intensity of the incident electromagnetic wave is expressed by the magnitude of the poynting vector. The magnitude of the poynting vector is defined as

$$S = \frac{1}{\mu_0} \cdot \frac{n_{\text{out}}}{c} \cdot |\mathbf{E_0}|^2.$$

Here, $\mu_0 = (c^2 \cdot \varepsilon_0)$, yielding

$$S = n_{\text{out}} \cdot c \cdot \varepsilon_0 \cdot |\mathbf{E_0}|^2.$$

The intensity of the incident electromagnetic wave is equal to the time averaged magnitude of the poynting vector. The only thing varying is the amplitude of the external E-field $\mathbf{E_0}$, yielding

$$\langle S \rangle = \frac{1}{2} \cdot n_{\text{out}} \cdot c \cdot \varepsilon_0 \cdot |\mathbf{E_0}|^2 = I_0. \tag{4.16}$$

4.1.5 Absorption Cross-section

Lastly, the absorption cross-section can be expressed for a spherical nanoparticle by equation (4.15) and (4.16), giving

$$\sigma_{\text{abs}} = \frac{\frac{V}{2} \cdot \omega \cdot \varepsilon_0 \cdot \Im(\varepsilon_{\text{eff}}) \cdot \frac{9 \cdot \varepsilon_{\text{out}}^2}{|\varepsilon_{\text{eff}} + 2\varepsilon_{\text{out}}|^2} \cdot |\mathbf{E_0}|^2}{\frac{1}{2} \cdot n_{\text{out}} \cdot c \cdot \varepsilon_0 \cdot |\mathbf{E_0}|^2} = \frac{\frac{V}{2} \cdot \omega \cdot \varepsilon_0 \cdot \Im(\varepsilon_{\text{eff}}) \cdot 9 \cdot \varepsilon_{\text{out}}^2 \cdot |\mathbf{E_0}|^2}{\frac{1}{2} \cdot n_{\text{out}} \cdot c \cdot \varepsilon_0 \cdot |\mathbf{E_0}|^2 \cdot |\varepsilon_{\text{eff}} + 2\varepsilon_{\text{out}}|^2}.$$

Simplifying and inserting $\frac{\omega}{c} = \frac{2\pi}{\lambda}$,$V = \frac{4}{3} \cdot \pi \cdot r_{\text{s}}^3$ and $n_{\text{out}} = \sqrt{\varepsilon_{\text{out}}}$,

$$\sigma_{\text{abs}} = \frac{24 \cdot \pi^2 \cdot r_{\text{s}}^3 \cdot \Im(\varepsilon_{\text{eff}}) \cdot \varepsilon_{\text{out}}^{\frac{3}{2}}}{\lambda \cdot |\varepsilon_{\text{eff}} + 2\varepsilon_{\text{out}}|^2}.$$

The nanoparticle is suspended in water, and thus the dielectric constant is $\varepsilon_{\text{out}} = n_{\text{water}}^2 = 1.33^2$. The dielectric constant of the nanoparticle can be described as $\varepsilon_{\text{eff}} = \varepsilon'_{\text{eff}} + i\varepsilon''_{\text{eff}}$ as it is complex, giving

$$\sigma_{\text{abs}} = \frac{24 \cdot \pi^2 \cdot r_s^3 \cdot 1.33^{\frac{3}{2}} \cdot \varepsilon''_{\text{eff}}}{\lambda \cdot (\varepsilon'_{\text{eff}} + 2 \cdot 1.33^2)^2 + (\varepsilon''_{\text{eff}})^2}. \tag{4.17}$$

The dielectric constant of a silver nanoparticle is $\varepsilon_{\text{eff}} = (n+ik)^2 = (n^2-k^2)+2ink$, where n^2-k^2 is the real part and $2nk$ is the imaginary part. n and k are specific for silver, and are determined experimentally and given in a database [44].

$$\sigma_{\text{abs}} = \frac{24 \cdot \pi^2 \cdot r_{\text{s}}^3 \cdot (1.33^2)^{\frac{3}{2}} \cdot 2 \cdot n \cdot k}{\lambda \cdot ((n^2-k^2)+2 \cdot 1.33^2)^2 + (2 \cdot n \cdot k)^2}. \tag{4.18}$$

Values for n and k were not given at every integer of wavelength, thus these values were determined by interpolation. The absorption cross-section is displayed as a function of the wavelength in Figure 4.3 with different radii of the SAgNP.

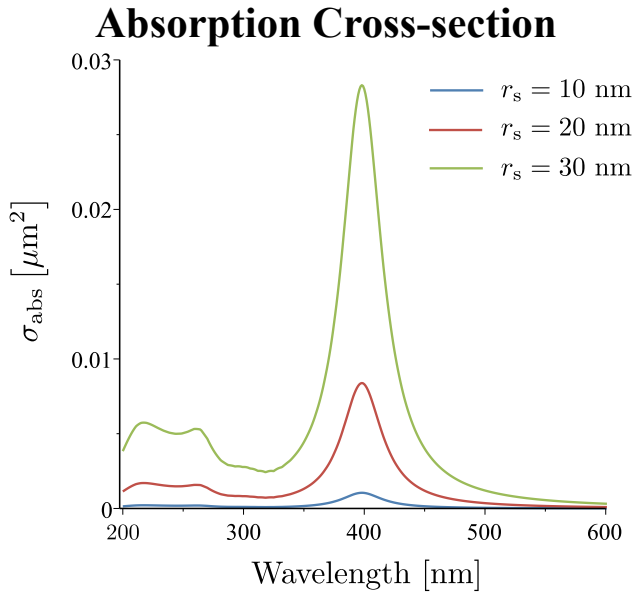

Figure 4.3. Plot displaying absorption cross-section at different wavelengths with maximum absorption at wavelength 397.33 nm. The absorbance increases with radius of the SAgNP, however, it does not shift the maximum absorption wavelength.

The maximum absorption wavelength is found to be at approximately 397.33 nm. As can be observed from Figure 4.3, the different radii of the SAgNP do not change λ_{max}, only the magnitude of the absorption cross-section.

4.2 Absorption of Triangular Silver Nanoprisms

TAgNPs have a higher antimicrobial effect, possibly due to the larger surface-to-volume ratio, see Section 4.5. The research into how to determine the shape of the AgNPs are of great importance.
TAgNPs have a higher percentage of {111} facets than spherical and rodlike AgNPs, and these facets are proposed to contribute significantly to the greater antimicrobial effect. Furthermore, these facets are a factor in how the absorption spectra of TAgNPs appear compared to SAgNPs which was shown in Figure 4.3. According to Mock *et al.*, there will be a maximum absorption wavelength ranging from 555 to 625 nm due to the triangular shape of the AgNPs. Unlike the SAgNPs, there is no clear correlation between the size of the TAgNPs and the maximum absorption wavelength according to Mock *et al.*, see Figure 4.4. [45]

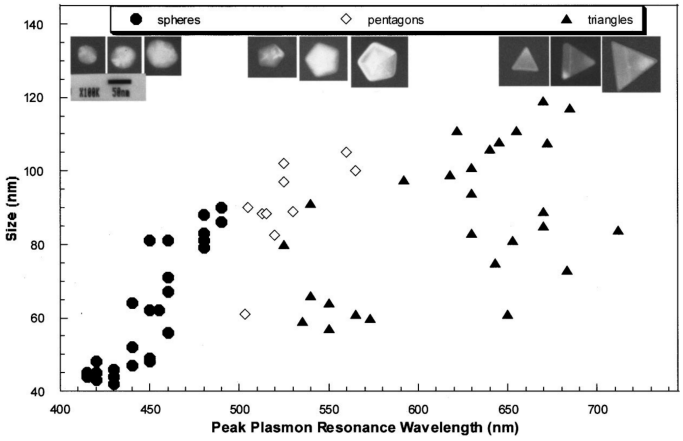

Figure 4.4. There is a clear correlation between size and peak of absorption in SAgNPs, where the maximum absorption wavelength is red-shifted as the size of the particles increase. In contrast, there is no clear correlation between size and maximum absorption wavelength in TAgNPs. [45]

The maximum absorption wavelength of TAgNPs is found to depend mainly on the roundness of the corners of the triangle, see Figure 4.5. Mock *et al.* have heated the TAgNPs, and measured the absorption spectra of them after 30 min, and after an additional 20 min. The corners were at their sharpest before being heated, and the maximum absorption wavelength was at 625 nm. After being heated for 30 min, the corners were softened a bit, and there was a blue-shift in the maximum absorption wavelength to 585 nm. After additional 20 min of heating, the edges of the triangles were at their softest, and the maximum absorption wavelength was at 555 nm, see Figure 4.5.

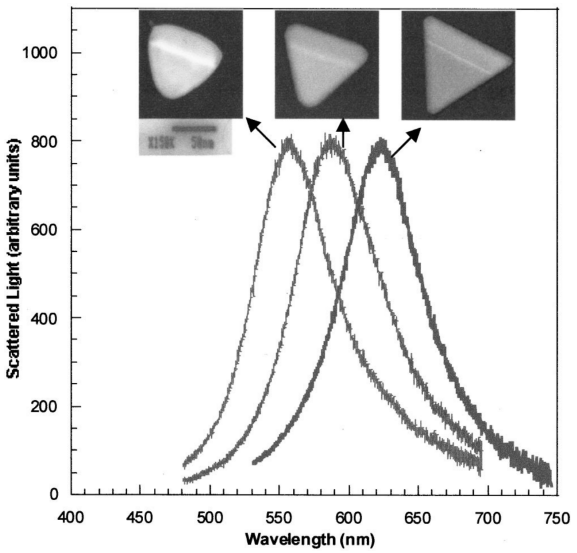

Figure 4.5. The wavelength of the maximum absorption of TAgNPs is mainly determined by the roundness of the corners. Sharp corners result in a red-shift in the maximum absorption wavelength. The sharp corners correspond to a maximum absorption wavelength at 625 nm, the softer edges at 585 nm, and the softest edges at 555 nm. [45]

Chen *et al.* found that their truncated TAgNPs had a maximum absorption wavelength at 552 nm, see Figure 4.7, and they had made very truncated TAgNPs, see Figure 4.6. [46]

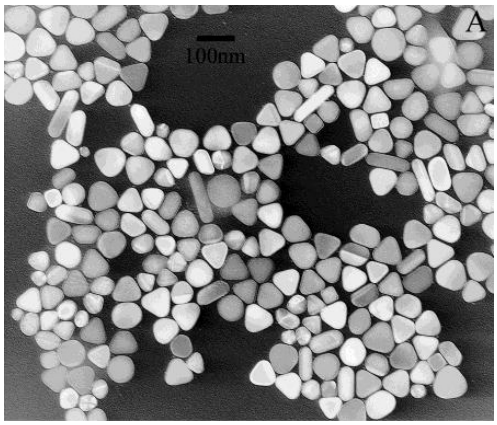

Figure 4.6. TEM picture showing truncated TAgNPs with very soft edges, which should, according to Mock *et al* [45], result in a blue-shift in maximum absorption wavelength.[46]

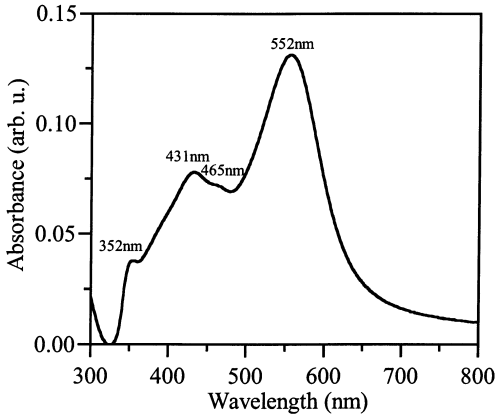

Figure 4.7. Absorption spectrum of the truncated TAgNPs shown in Figure 4.6, illustrating a maximum absorption wavelength at 552 nm, which corresponds with the wavelength Mock *et al.* [45] found for TAgNPs with truncated corners [46].

In line with the findings of Mock *et al.* [45] and Chen *et al.* [46], Jin *et al.* [47] found that the more truncated the TAgNPs were, the more blue-shifted their maximum absorption wavelength became, see Figure 4.8.

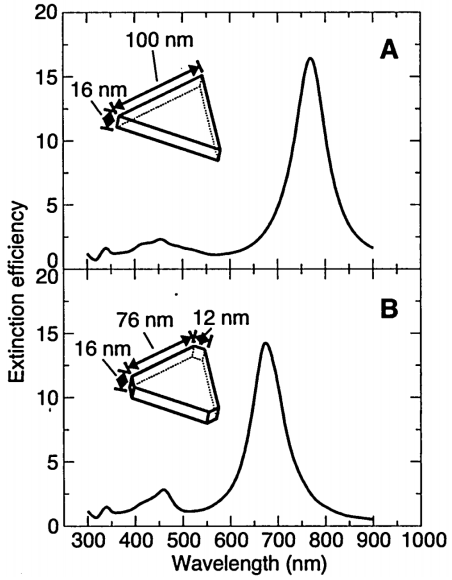

Figure 4.8. Illustration showing A) the absorption spectrum of sharp TAgNPs and B) the absorption spectrum of more truncated TAgNPs. The blue-shift in the maximum absorption wavelength is evident, as the TAgNPs becomes more truncated [45].

4.3 Synthesis of Spherical Silver Nanoparticles

The SAgNPs are synthesized using a chemical reduction method described by Mulfinger *et al.* [48]. Silver nitrate is slowly added to a solution of sodium borohydride, which acts as a reducing agent of silver nitrate into metallic silver. The nanoparticles produced in this

synthesis should be in the size range of 12 ± 2 nm.

$$AgNO_3 + NaBH_4 \longrightarrow Ag + \tfrac{1}{2}\,H_2 + \tfrac{1}{2}\,B_2H_6 + NaNO_3. \tag{4.19}$$

The borohydride ions also act as a stabilizing agent, and are adsorbed onto the SAgNPs giving them an overall negative surface charge and thereby creating electrostatic repulsion between the SAgNPs preventing further aggregation [48]. However, borohydride ions are unstable in water, and will react with water to form boric acid over time. Boric acid is moderately soluble in water and will act as a weak Lewis acid towards OH^- [49, 50].

$$BH_4^- + 4\,H_2O \longrightarrow B(OH)_3 + OH^- + 4\,H_2 \longrightarrow B(OH)_4^- + 4\,H_2 \tag{4.20}$$

The boric acid ions will, however, act as a stabilizing agent in the same way as borohydride ions. However, if electrolytes such as sodium chloride is added to the solution the charges on the surface of the SAgNPs will be shielded, and the SAgNPs will be allowed to aggregate. [48]
Since the antimicrobial effect of the nanoparticles in this project will be tested in a broth bacterial culture, containing sodium chloride, sodium borohydride will not be sufficient as a stabilizing agent. As a stabilizing agent polysorbate 80 (Tween 80), which is a surfactant, can be used. Tween 80 will be adsorbed onto the SAgNPs and prevent aggregation of the nanoparticles due to steric hindrance, even when in the presence of electrolytes. [48, 51]

4.4 Synthesis of Triangular Silver Nanoprisms

There are several ways to synthesize TAgNPs, and in this project, the most simple one is chosen, which is a chemical reduction synthesis. Firstly, seed AgNPs are produced by reduction of silver ions to metallic silver by sodium borohydride in a solution with trisodium citrate and poly(sodium styrene sulphonate). The trisodium citrate acts as a reducing agent like sodium borohydride, though mainly as a stabilizer because of its three carboxylate ion groups, when deprotonated. To stabilize, trisodium citrate binds one ionized carboxylate group to the surface of the seed nanoparticles, while the two remaining ionized carboxylate groups are free to act as electrostatic hindrance between the seed nanoparticles in the solution ensuring no further aggregation [52]. By adding a surfactant or polymer, here poly(sodium styrene sulphonate), see Figure 4.9, one can control the properties of the seed particles and prevent a diverse seed solution, where some seeds might grow into spheres and some might grow into prisms.

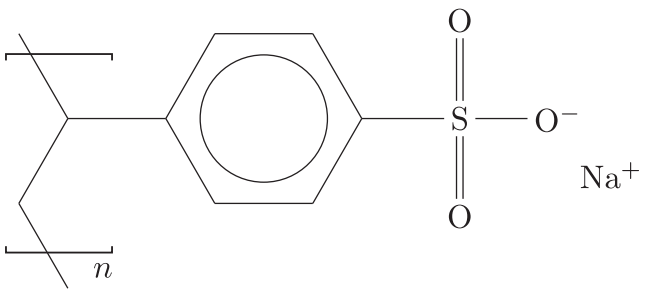

Figure 4.9. Chemical representation of the surfactant poly(sodium styrene sulphonate).

The polymer or surfactant creates a micelle around the seed particles, and poly(sodium styrene sulphonate) creates a rodlike micelle, ensuring only prisms are formed. Lastly, trisodium citrate is added to the solution in order to stabilize the seed particles. The reaction is carried out at room temperature, where sodium borohydride reduces silver ions at a high rate, forming a large amount of very small seed particles. Sodium borohydride is the primary reducing agent as it reacts faster than the trisodium citrate.
The stabilized seed particles are diluted in a solution of ascorbic acid and water, where ascorbic acid acts as primary reducing agent. By slowly adding silver nitrate, the metallic silver will aggregate upon the seed particles into a crystal structure. The silver crystal structure is growing inside the micelle structure, which acts as a limiting agent in the [111] direction, see Figure 4.10.

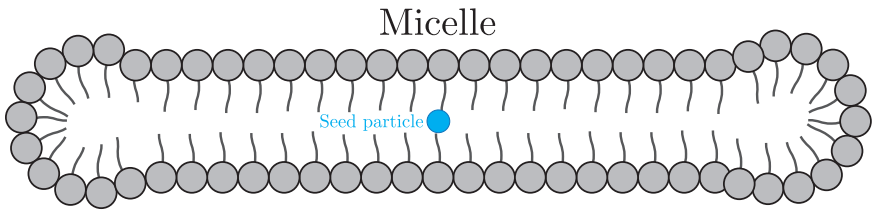

Figure 4.10. Illustration of the micelle containing the silver seed particle, limiting growth to only two dimensions.

The slow rate of silver nitrate results in a fast growth in the easily accessible plane perpendicular to the [111] direction, resulting in a flat triangular silver nanoprism, see Figure 4.11. However, the growth parameters of seed nanoparticles are not yet fully understood [53].
Lastly trisodium citrate is added once more to the solution to stabilize the grown TAgNPs preventing further aggregation. [54]

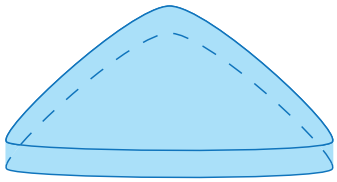

Figure 4.11. Illustration of the structure of a produced TAgNP, whose growth in the [111] direction has been limited during the synthesis.

4.5 Antimicrobial Properties of Silver Nanoparticles

There are a large number of proposed mechanisms, through which AgNPs inhibit or reduce bacterial cell growth and metabolism resulting in accelerated cell lysis or population growth plateau. However, this project will only concern the uptake of free silver ions by bacterial cells disrupting the ATP production, generation of reactive oxygen species (ROS) by both AgNPs and silver ions, and by direct damage to bacterial cells by AgNPs. [55]

4.5.1 Free Silver Ions

Silver ions are potentially very reactive, and can react with the negatively charged cell membrane. The release of silver ions from AgNPs avoids the use of silver salts in treatments, and AgNPs are furthermore, less susceptible to deactivation by chloride ions in physiological media compared to silver salts. AgNPs offer a slow and controlled release of silver ions compared to reactive silver salts making them more desirable in treatments. [12]

In certain solutions and situations, AgNPs posses the same intrinsic antimicrobial properties, since they can potentially dissolve and generate free silver ions from their surfaces. Silver ions are produced by AgNPs, when the silver is oxidized by strong oxidants, and Morones *et al.* found that when 0.7 mM silver, in the form of AgNPs, were dissolved in 0.2 M sodium nitrate, they rapidly released ions in the concentration of 1 μM. The concentration of ions decreased to < 0.2 μM due to aggregation of ions onto existing or into new nanoparticles over time [56]. There are different proposed mechanisms through which the ions are released, and one proposed reaction is the reaction between the nanoparticles, hydrogen peroxide, and two protons [57]:

$$2\,\mathrm{Ag} + \mathrm{H_2O_2} + 2\,\mathrm{H^+} \longrightarrow 2\,\mathrm{Ag^+} + 2\,\mathrm{H_2O}. \tag{4.21}$$

For Reaction (4.21) to occur, there must be peroxides present prior to the production of silver ions. A mechanism proposed by Liu *et al.*, however, should be able to take place as long as oxygen and water is present [58]:

$$4\,\mathrm{Ag} + \mathrm{O_2} + 2\,\mathrm{H^+} \longleftrightarrow 2\,\mathrm{Ag^+} + \mathrm{H_2O}. \tag{4.22}$$

They showed, that under aerobic conditions, AgNPs suspended in deionized water will produce silver ions, while this is not the case in anaerobic conditions. Even polymeric stabilizers did not protect the AgNPs against the ion release. The experiment, however, shows that the pH value of the solution has an important role to play in the production of ions, and a pH 4 is the optimal value for ion formation, see Figure 4.12.

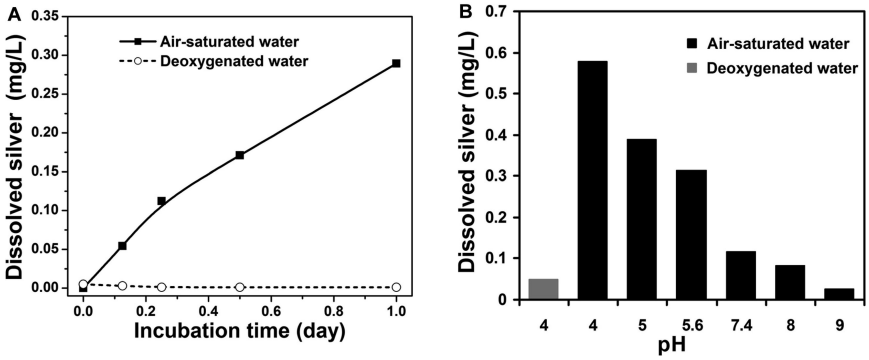

Figure 4.12. Two graphs showing A) the formation of silver ions in air-saturated water over time and B) the effect of the pH value of the water [58].

The antimicrobial effects of this hypothesis was tested by Xiu *et al.*, who tested the bactericidal effects of AgNPs under both aerobic and anaerobic conditions. They found, that there was no bactericidal effect of the AgNPs under anaerobic conditions, even at high concentrations of AgNPs. They suggest that the particles themselves have no bactericidal effect, and that silver ions cannot be released in the absence of oxygen. Furthermore, locally in the periplasmic place pH is as low as 3.0 due to the proton motive force (PMF) and free protons, which will enhance silver ion release from the AgNPs. [59]
However, one could argue that this does not exclude any other bactericidal effect of AgNPs beside the release of ions. Xiu *et al.* have carried out their experiments on *E. coli*, which is an facultative anaerobic bacteria, meaning that during anaerobic conditions the final electron acceptor is some nonoxygenic compound, and there is no natural production of ROS during anaerobic respiration. AgNPs are stated to react with enzymes processing ROS, resulting in an increase in ROS levels, which is cytotoxic. However, if there is no neutral production of ROS in the first place, due to anaerobic conditions, the inhibitory effect of the AgNPs is negligible since the ROS levels wil not increase, thus no bactericidal effect will appear during anaerobic conditions.
The antimicrobial effects of silver ions are well documented. The silver ions can interact with enzymes participating in the respiratory reactions of the bacteria, resulting in a breakdown of the synthesis of ATP [60, 61, 62, 63]. Furthermore, silver ions can bond to the specialized carrier proteins and enzymes residing in the bacterial cell membrane. This chain of proteins and enzymes transport electrons and simultaneously move protons from the cytoplasm into the periplasmic space creating a concentration gradient termed the PMF. This electron transport system over the cell membrane is the primary generator of ATP during aerobic respiration in bacteria, and the process is termed chemiosmosis. The only place protons can diffuse into the cytoplasm again is through the ATP synthase complex, which results in the formation of ATP by a redox reaction between ADP and inorganic phosphate, and the electrons reaching the final electron acceptor site, see Figure 4.13. The final electron acceptor is dissolved oxygen in the case of aerobic respiration, and primarily results in water or in small concentrations of cytotoxic ROSs, which specialized enzymes process.
The bonding of silver ions to the carrier proteins and enzymes, crucial to the ATP generation, leads to a proton leakage inducing a collapse of the PMF resulting in a halt of the ATP synthesis and induces bacterial lysis. [3, 64]

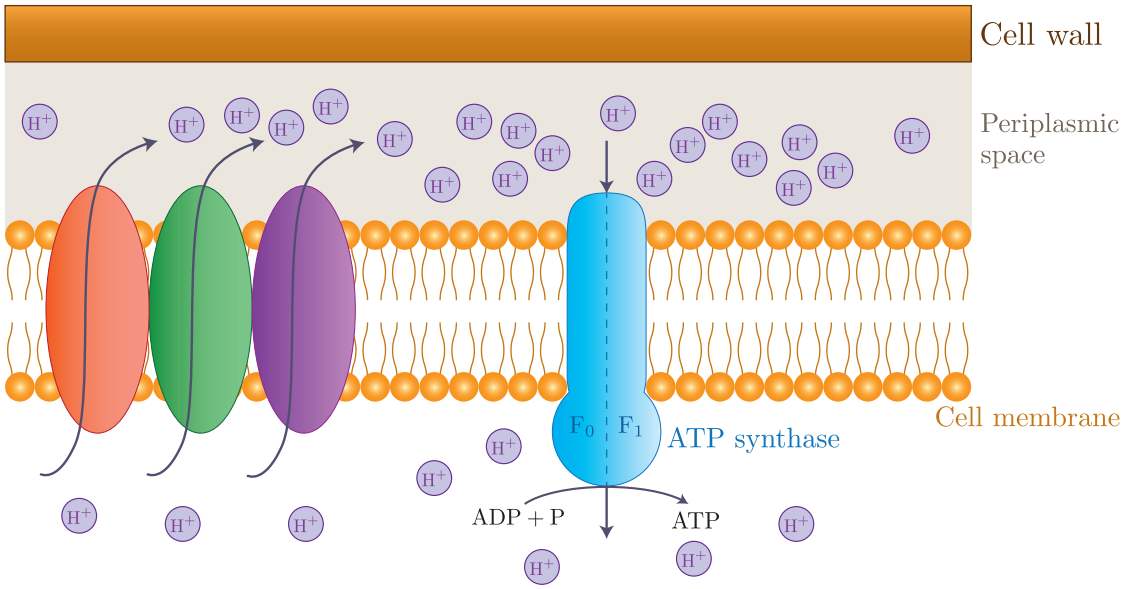

Figure 4.13. The PMF occurs over the cell membrane in bacteria. ATP synthase is a complex enzyme composed of two primary units, F_0 and F_1, and as protons diffuse through the F_0 center, the F_1 center pulls in ADP and inorganic phosphate. ATP synthase then rotates its motoric parts, which creates a high-energy bond between ADP and the third phosphate, forming ATP. The ATP is released into the cytoplasm and ATP synthase rotates back to original position ready to repeat the reaction. When electron transport and ATP synthesis is linked together, the ATP is formed by oxidative phosphorylation. Lastly the protons reach the last electron donor site, which in the case of aerobic respiration is oxygen. The ATP molecules are used by the cell to carry out synthesis reactions. As an example, the bacterium *E. coli* consumes around 2.5 million ATP molecules pr. second for synthesis alone. [3]

Feng *et al.* and Jung *et al.* have shown that silver ions are capable of disturbing the electron density within the bacteria, as well as creating a new large gab between the cell membrane and the cell wall [65, 66]. Furthermore, it was shown that the cell membrane sometimes completely dissolves, which leads to intracellular leakage. Silver ions have also been shown to bond with DNA molecules in the cells, thus causing mutations [67]. Although there is a shown antimicrobial effect of the silver ions, some cells go into an *active but not cultivable* state. In this state, the bacteria are physiologically alive, but there is no detectable growth and thus the bacteria are not cultivable.
As it has been described in this section, silver ions are highly toxic to cells, and it has been proposed that production of ions is one of the main causes of the bactericidal effect of AgNPs [57, 64, 68]. It is however evident, from the reactions proposed by Liu *et al.* and Morones *et al.*, that either an oxidizing or acidic environment needs to be present before the formation of silver ions can occur. The formation of ROS, such as hydrogen peroxide is also a complex process which is not well understood.

4.5.2 Reactive Oxygen Species

ROS are a group of highly reactive and short lived oxidants. ROS include molecules such as hydrogen peroxide (H_2O_2), superoxide radicals (O_2^-), singlet oxygens (O_2), and hydroxyl radicals ($\cdot OH$) [55, 69]. ROS are widely used in antibiotics and other drugs designed to kill bacteria [69].

The metabolism of any aerobe respiring organism produces small concentrations of ROS that are very toxic to the organisms. However, every aerobic organism posses the necessary enzymatic antioxidant defences to process these cytotoxins. Further generation of ROS can lead to oxidative stress in the cell, and eventually cell death [3, 70], and ROS can attack proteins, membrane lipids, and DNA in the cell [71].
Carlson *et al.* have studied the formation of ROS as a result of AgNPs, and found that the use of AgNPs of 15 nm resulted in a decreased level of the important antioxidant Glutathione entailing weakening of the antioxidant defence of the cell and an increase of ROS levels [72]. Moreover, one could hypothesize that the created oxidizing intracellular environment would lead to oxidation of AgNPs releasing silver ions, see Equation (4.21).
Kim *et al.* used the antioxidant N-acetyl-cysteine along with AgNPs in order to determine if ROS had any influence on the antimicrobial effects of the nanoparticles, which was found to be the case [10]. Complementary, other studies have reported an increase in ROS as a result of the presence of either AgNPs or silver ions [56, 73].
The antimicrobial effects of silver ions have been described, but their contribution to the formation of ROS should also be noted. Park *et al.* and Hwang *et al.* have reported that silver ions are responsible for a part of the formation of ROS, and they found that the main oxygen species formed was the superoxide radical. Furthermore, they found that the generation of superoxide radicals was closely related to the reaction between the silver ions and the enzymes of the respiratory pathways. [69, 74]

4.5.3 Direct Cell Damage by Silver Nanoparticles

Choi *et al.*, Raffi *et al.*, Sondi *et al.*, and Smetana *et al.* have all reported that AgNPs are capable of attaching themselves to the bacterial cell wall and membrane and changing the permeability, resulting in both membrane and wall penetration of the cell [68, 75, 76, 77, 78]. Li *et al.* showed with TEM how the AgNPs attach themselves to the cell membrane of *E. coli* and enter the cell, see Figure 4.14.

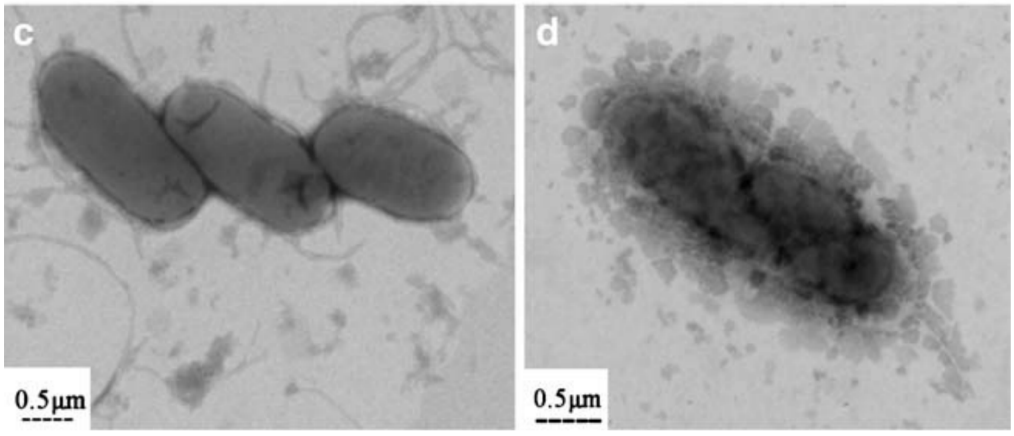

Figure 4.14. TEM pictures showing c) *E. coli* untreated and d) *E coli* treated with AgNPs. It is clearly seen, that the AgNPs attach themselves to the cell membrane and enter the cell. [79]

The change in permeability of the membrane and wall is supposed to originate in a release of both wall and membrane proteins and a degradation of the outer membrane layer in gram-negative bacteria [55, 80]. Furthermore, wall and membrane disruption, as a result of AgNP

accumulation have been reported, disturbing the membrane integrity. This contributes to the ability of the particles to enter the cell freely. The AgNPs are suspected to disrupt gradients of the cell membrane such as the PMF and potassium and sodium gradients by leakage of intracellular components due to competitive inhabitation of transport proteins crucial to the gradient maintenance or cell wall gaps. [55, 77]
Several sulphur compounds reside in the bacterium membrane of gram-negative bacteria [3], and the PG cell wall consists primarily of teichoic and lipoteichoic acid, which are phosphorus molecules. Moreover, the bacterial membrane consists of phospholipids. Silver is very reactive towards sulphur and phosphorus when in contact [56], and this is speculated to be the mechanism through which, the AgNPs disturb the membrane and wall integrity of the bacteria. Data obtained with TEM show that AgNPs are capable of entering bacteria, and once inside, the AgNPs will have a tendency to react with other phosphorus and sulphur compounds such as proteins and DNA. There is no definitive conclusion to these speculations, and Morones *et al.* and Hwang *et al.* found no induced DNA damage caused by AgNPs, but only damage done to proteins and the cell membrane [56, 74]. This is supported by Gogoi *et al.* who found that DNA from *E. coli* treated with AgNPs did not show any alteration [81].
Studies using different ligands and surfactants for stabilizing the nanoparticles have found that some surfactants increase the bactericidal effects such as positively charged stabilizers [51, 82, 83], while others have the opposite antimicrobial effects like negatively charged stabilizers [77]. Furthermore, some stabilizers remain neutral in terms of antimicrobial effect.

4.5.4 Size and Shape of the Silver Nanoparticles

It is widely accepted that the size and shape of the nanoparticles greatly influence the antimicrobial effect of the particles [84]. A larger surface-to-volume ratio results in a higher concentration of silver ions released during suspension of particles, and a higher degree of silver is able to react with the cell wall and membrane. Futhermore, smaller particles can have a higher affinity for entering the bacteria.
Crystal facets {111} and {100} are responsible for the reactivity of AgNPs. TAgNPs predominantly have {111} rather than {100} facets, and spherical and rodlike AgNPs predominantly have {100} facets. The {111} facet has a higher atomic density resulting in increased binding efficiency of silver to sulphur and phosphorus, making the TAgNPs more effective than their spherical and rodlike counterparts [8, 55, 56, 84]. Furthermore, TAgNPs have a higher surface-to-volume ratio compared to spherical or rodlike AgNPs resulting in a higher antimicrobial effect. [55, 56, 72, 84]

5. Materials and Methods

This chapter presents the synthesis method of silver ions, SAgNPs, and TAgNPs. The characterization method of the AgNPs and the determination method of the bactericidal effect of the antimicrobial agents toward *E. coli* and *B. subtilis* will lastly be described.

5.1 Synthesis of Silver Ions

Materials

- 250 mL Bluecap container for $AgNO_3$ solution

Chemicals

- 10 mM $AgNO_3$ ($\geq$ 99.8 %) stock solution (VWR International)
- Milli-Q water

Two concentrations of silver ions were made, corresponding to the concentrations of silver in the SAgNP solutions. This resulted in two silver ion solutions of 0.74 mM and 2.16 mM. The silver cations were prepared by dissolving silver nitrate ($AgNO_3$) in Milli-Q water producing silver cations and nitrate anions. To minimize waste, the $AgNO_3$ solution from synthesis of AgNPs was diluted in Milli-Q water until the concentrations of 0.74 mM and 2.16 mM were reached.

5.2 Synthesis of Spherical Silver Nanoparticles

Materials

- Magnetic stirrer with magnets
- 250 mL Bluecap container for $AgNO_3$ stock solution
- 500 mL Bluecap container for $NaBH_4$ stock solution
- 50 mL Bluecap container for SAgNP solution
- 25 mL Bluecap container for SAgNP solution
- 1 - 5 mL Eppendorf pipette
- 10 mL Volumetric pipettes
- Plastic pasteur pipettes
- Ice

Chemicals

- 10 mM $AgNO_3$ ($\geq$ 99.8 %) stock solution (VWR International)
- 20 mM $NaBH_4$ ($\geq$ 98 %) stock solution (Sigma Aldrich)
- Tween 80 (Sigma Aldrich)
- Milli-Q water

Firstly, $AgNO_3$ and sodium borohydride ($NaBH_4$) was dissolved in Milli-Q water resulting in two stock solutions of 10 mM and 20 mM, respectively. In order to synthesize SAgNPs, $AgNO_3$ was reduced by $NaBH_4$ while being stirred on ice, which resulted in a 0.6 mM and a 2.0 mM SAgNP solution. The 0.6 mM SAgNP solution was synthesized by stirring 30 mL $NaBH_4$ stock on ice for 20 minutes. Afterwards, 2 mL $AgNO_3$ stock was added at a

rate of one drop per second. This resulted in a brownish solution of SAgNPs. To stabilize the SAgNPs, 600 µL Tween 80 was added to the solution, supplying steric hindrance, immediately after the last drop of $AgNO_3$. The solution was taken off the ice and magnetic stirrer, and Tween 80 would fully dissolve.
For the 2.0 mM SAgNP solution, the same procedure was used, but with 15 mL $NaBH_4$ stock and 4 mL $AgNO_3$ stock. When adding Tween 80 into both solutions, the Eppendorf pipette was set to 1 mL, but due to the viscosity of Tween 80, not all was emptied from the pipette tip. Due to this, approximately 500 - 600 µL was added to the solutions.
The SAgNP solutions were stored in darkness at 3.4 °C.

5.3 Synthesis of Triangular Silver Nanoprisms

Materials

- Magnetic stirrer with magnets
- 12 mL disposable glas flasks for stock solutions, seed stock solution, and finished TAgNP solutions
- 50 mL Bluecap container for $AgNO_3$ stock solution
- 10 - 100 µL Eppendorf pipette
- 100 - 1000 µL Eppendorf pipette
- 1 - 5 mL Eppendorf pipette
- 10 mL Volumetric pipettes
- Plastic pasteur pipettes

Chemicals

- 10 mM $AgNO_3$ ($\geq$ 99.8 %) stock solution (VWR International)
- 25 mM and 2.5 mM $C_6H_5O_7 \cdot 3\,Na$ ($\geq$ 99.5 %) stock solution (Sigma Aldrich)
- 20 mM $NaBH_4$ ($\geq$ 98 %) stock solution (Sigma Aldrich)
- 500 mg/L $[C_8H_7NaO_3S]n$ (Sigma Aldrich)
- 10 mM $C_6H_8O_6$ ($\geq$ 99.7 %) stock solution (Sigma Aldrich)
- Milli-Q water

Firstly, $AgNO_3$ and $NaBH_4$ was dissolved in Milli-Q water resulting in two stock solutions of 10 mM and 20 mM, respectively.
In order to synthesize TAgNPs one will need a silver seed particle solution. Silver nano seed particles were prepared by reducing $AgNO_3$ with $NaBH_4$ in the presence of trisodium citrate ($C_6H_5O_7 \cdot 3\,Na$) and poly(sodium styrene sulphonate) ($[C_8H_7NaO_3S]n$). 5 mL 2.5 mM $C_6H_5O_7 \cdot 3\,Na$ and 0.25 mL 500 mg/L $[C_8H_7NaO_3S]n$ was mixed together. While stirring, 0.3 mL 10 mM $NaBH_4$ was slowly added to the solution, and 5 mL 0.5 mM $AgNO_3$ was added at a rate of 2 mL per minute resulting in a yellow seed stock solution.
In order to synthesize a 0.17 mM TAgNP solution, 75 µL 10 mM ascorbic acid ($C_6H_8O_6$) was dissolved into 5 mL Milli-Q water, and 150 µL seed stock solution was slowly added to this solution. Afterwards, 3 mL 0.5 mM $AgNO_3$ was added at a rate of 1 mL per minute resulting in a deep blue solution of TAgNPs. The TAgNPs were stabilized by 0.5 mL 25 mM $C_6H_5O_7 \cdot 3\,Na$ supplying electrostatic repulsion between particles. The procedure was repeated ten times to produce enough TAgNP solution for the experiments. The TAgNP solutions were stored in darkness at 3.4 °C.

5.4 Characterization of Silver Nanoparticles

In order to determine the size and shape of the produced nanoparticles, two methods have been used; absorption spectroscopy and AFM.
AFM was carried out by applying a droplet of a AgNP solution to a clean mica plate. The

droplet was then left for drying before performing AFM measurements in dynamic mode on the sample. This resulted in a visualized morphology of the produced nanoparticles.
Absorption spectroscopy was performed by adding 1 mL of the AgNP solutions to a semi micro cuvette. Using a UV1 UV/visible spectrophotometer from VWR International along with the software VisionLite Scan, the absorption of the AgNP solutions was measured from a wavelength of 300 to 800 nm with an interval of one nm. This resulted in a specific spectrum for each nanoparticle solution.

5.5 Bactericidal Effect of Silver Nanoparticles

The bactericidal effect of AgNPs and silver ions were tested on two bacteria grown in broths; *B. subtilis* and *E. coli*. The following section contains two method subsections, one for each bacteria.

5.5.1 *Bacillus subtilis*

Materials
- 1000 mL Erlenmeyer flasks for broth YP
- 500 mL Bluecap container for extra broth YP
- 500 mL Bluecap container for agar media
- Sterile Petri dishes for agar plates
- Sterile 12 mL culture tubes
- Sterile inoculating loops
- Semi micro cuvettes
- Magnetic stirrer with magnets
- Bunsen burner
- Sterile Drigalski spatula
- 1 - 5 mL Eppendorf pipette
- 100 - 1000 µL Eppendorf pipette
- Autoclave from JP Selecta
- Innova 4230 Refrigerated Incubator Shaker from New Brunswick Scientific
- Ultrospec 3000 UV/Visible spectrophotometer from Pharmacia Biotech

Chemicals
- 5 g/L Tryptone (Applichem)
- 5 g/L Yeast extract (Fermtech)
- 15 g/L Agar (Sigma Aldrich)
- Milli-Q water
- *Bacillus subtilis* strain DSM2 2109
- 0.9 % NaCl solution

In order to test the bactericidal effect of AgNPs and silver ions, *B. subtilis* cells were grown on Yeast Peptone (YP) agar plates. The agar plates were prepared by dissolving 5 g/L tryptone, 5 g/L yeast extract, and 15 g/L agar-agar in Milli-Q water. The agar medium was prepared in Bluecap bottles containing a magnet for later stirring.
Broth YP was prepared by dissolving 5 g/L tryptone and 5 g/L yeast extract in Milli-Q water. The broths were prepared in 1000 mL Erlenmeyer flasks in portions of 100 mL. Additional medium for dilution and reference was prepared in a 500 mL Bluecap container. Physiological salt was prepared by dissolving sodium chloride (NaCl) in Milli-Q water.
The different YP media and the physiological salt solution were autoclaved at 121 °C, 1 bar above the atmospheric pressure for 30 minutes along with pipette tips.

After autoclaving, the YP agar media were slowly cooled down while being stirred with a magnetic stirrer, to ensure an even cooling. Before the agar media hardened, it was poured into Petri dishes to 3 - 5 mm height. When the plates had hardened *B. subtilis* cells were added onto the YP agar plates using a Drigalski spatula. This was done in the presence of a lit Bunsen burner in order to create an upward airflow to prevent contamination of the plates. The agar plates with bacterial cells were placed at 37 °C for about a day to allow growth of the bacteria. The rest of the solutions were placed in the refrigerator at 3.4 °C along with the agar plates when a sufficient amount of bacteria had grown on them, while the sterile pipette tips were placed at 60 °C. When the amount of bacteria was running low, some bacterial cells were transferred to new agar plates and allowed to grow again.
The bactericidal effect of the antimicrobial agents was tested in the broths. Firstly, a preculture was prepared by adding 5 mL YP broth to a sterile culture tube, and placing bacterial cells from the agar plates into the culture tube using a sterile inoculating loop in the presence of a lit Bunsen burner. The preculture was placed in an incubator shaker at 37 °C and shaken with 230 rpm over night. New precultures were made fresh before each experiment.
In order to determine when the antimicrobial agents should be suspended in the bacterial culture, a standard growth curve was made. 2 mL of three different precultures were suspended into three 1000 mL Erlenmeyer flasks containing 100 mL broth. The cultures where placed in an incubator shaker at 37 °C and 230 rpm. The bacterial growth was determined by measuring the OD_{600} of the cultures every 30 - 60 minutes with a spectrophotometer.
When the OD_{600} reached 0.7, the samples taken for measurement were diluted with extra YP broth in order to keep the measurements precise. This was done in the presence of a lit Bunsen burner, and bottlenecks were burned before and after a sample had been taken out of the Erlenmeyer flasks, to prevent contamination of the culture.
In order to determine the bactericidal effect of the AgNPs and silver ions, 1.5 mL of the same preculture was suspended in three 1000 mL Erlenmeyer flasks containing 100 mL YP broth. The same preculture was used, in order to minimize deviations.
When the OD_{600} had reached 0.7, 15 mL AgNP or silver ions solution were added to two of the cultures and 15 mL physiological salt was added to the last culture as a reference. The bacterial growth was determined by measuring the OD_{600} of the cultures every 30 - 60 minutes with a spectrophotometer, and the samples were diluted when OD_{600} reached 0.7.
Different concentrations of AgNPs and silver ions were used in these experiments. One concentration of one antimicrobial agent was used in one experiment. The final concentrations of silver in the cultures were 0.083 mM and 0.276 mM for SAgNPs, 0.024 mM for TAgNPs, and 0.103 mM and 0.298 mM for silver ions.
Absorption of the physiological salt and silver solutions at concentrations similar to those in the culture were measured relatively to Milli-Q water or the media in the culture was measured. This was done in order to correct any difference in OD_{600} measurements between salt and silver causing an unwanted deviation between the culture with the salt solution and the cultures with the silver solutions.

5.5.2 *Escherichia coli*

Materials

- 500 mL Erlenmeyer flasks for broth LB
- 500 mL Bluecap container for extra broth LB
- 500 mL Bluecap container for agar media
- Sterile Petri dishes for agar plates
- Sterile 12 mL culture tubes
- Sterile inoculating loops
- Semi micro cuvettes
- Magnetic stirrer with magnets
- Bunsen burner
- Sterile Drigalski spatula
- 1 - 5 mL Eppendorf pipette
- 100 - 1000 µL Eppendorf pipette
- Autoclave from JP Selecta
- Innova 4230 Refrigerated Incubator Shaker from New Brunswick Scientific
- UV1 UV/Visible spectrophotometer from VWR International including Visionlite Fixed software

Chemicals

- 10 g/L Tryptone (Applichem)
- 5 g/L Yeast extract (Fermtech)
- 5 g/L NaCl (Supplier Unknown)
- 15 g/L Agar (Sigma Aldrich)
- Milli-Q water
- *Escherichia coli* strain BL21 (DE3)
- 0.9 % NaCl solution

In order to test the bactericidal effect of AgNPs and silver ions, *E. coli* cells were grown onto LB agar plates. The agar plates were prepared by dissolving 10 g/L tryptone, 5 g/L yeast extract, 5 g/L NaCl, and 15 g/L agar-agar in Milli-Q water. The agar medium was prepared in Bluecap bottles containing a magnet for later stirring.
Broth LB was prepared by dissolving 10 g/L tryptone, 5 g/L NaCl, and 5 g/L yeast extract in Milli-Q water. The broths were prepared in 500 mL Erlenmeyer flasks in portions of 100 mL. Some additional media for dilution and reference were prepared in a 500 mL Bluecap container. Physiological salt was prepared by dissolving NaCl in Milli-Q water.
The different LB media and the physiological salt solution were autoclaved at 121 °C, 1 bar above atmospheric pressure for 30 minutes along with pipette tips.
After autoclaving, the LB agar media were slowly cooled down while being stirred with a magnetic stirrer, to ensure an even cooling. Before the agar media hardened, it was poured into Petri dishes to 3 - 5 mm height. When the plates had hardened *E. coli* cells were added on the LB agar plates using a sterile Drigalski spatula. This was done in the presence of a lit Bunsen burner in order to create an upward airflow to prevent contamination of the plates. The agar plates with bacterial cells were placed at 37 °C for about a day to allow growth of the bacteria. The rest of the solutions were placed in the refrigerator at 3.4 °C along with the agar plates when a sufficient amount of bacteria had grown on them, while the sterile pipette tips were placed at 60 °C. When the amount of bacteria was running low, some bacterial cells were transferred to new agar plates and allowed to grow again.
The bactericidal effect of the antimicrobial agents was tested in the broths. Firstly, a preculture was prepared by adding 5 mL LB broth to a sterile culture tube, and placing bacterial cells from the agar plates into the culture tube using a sterile inoculating loop in the presence of a lit Bunsen burner. The preculture was placed in an incubator shaker at

37 °C and shaken with 230 rpm over night. New precultures were made fresh before each experiment.
In order to determine when the antimicrobial agents should be suspended in the bacterial culture, a standard growth curve was made. 2 mL of three different precultures were suspended into three 500 mL Erlenmeyer flasks containing 100 mL broth. The cultures were placed in an incubator shaker at 37 °C and 230 rpm. The bacterial growth was determined by measuring the OD_{600} of the cultures every 30 - 60 minutes with a spectrophotometer. When the OD_{600} reached 0.7 the samples taken for measurement were diluted with extra LB broth in order to keep the measurements precise. This was done in the presence of a lit Bunsen burner, and bottlenecks were burned before and after a sample had been taken out of the Erlenmeyer flasks, to prevent contamination of the culture.
In order to determine the bactericidal effect of the AgNPs and silver ions, 1.5 mL of the same preculture was suspended into three 500 mL Erlenmeyer flasks containing 100 mL broth LB. This was done in order to minimize deviations.
When the OD_{600} had reached 0.7, 15 mL AgNP or silver ion solutions were added to two of the cultures and 15 mL physiological salt to the last culture as a reference. The bacterial growth was determined by measuring the OD_{600} of the cultures every 30 - 60 minutes with a spectrophotometer, and the samples were diluted when OD_{600} reached 0.7.
Different concentrations of AgNPs and silver ions were used in these experiments. One concentration of one antimicrobial agent was used in one experiment. The final concentrations of silver in the cultures were 0.083 mM and 0.273 mM for SAgNPs, 0.024 mM for TAgNPs, and 0.101 mM and 0.295 mM for silver ions.
Absorption of the physiological salt and silver solutions at concentrations similar to those in the culture were measured relatively to Milli-Q water or the media in the culture was measured. This was done in order to correct any difference in OD_{600} measurements between salt and silver causing an unwanted deviation between the culture with the salt solution and the cultures with the silver solutions.

6. Results

6.1 Characterisation of Silver Nanoparticles

To determine if the particles were actual AgNPs, absorption spectroscopy was used to determine if the experimental maximum absorption wavelength was identical to the theoretical one. The absorption was measured from 300 to 800 nm with an interval of 1 nm. To determine the size of the AgNPs, AFM measurement was used in dynamic mode. Note that all concentrations relating AgNPs or ions in this chapter are concentrations of the amount of silver atoms in the solutions.

6.1.1 Spherical Silver Nanoparticles

After the synthesis, 1 mL of each solution containing the assumed SAgNPs were tested by absorption spectroscopy yielding the absorption graphs shown in Figures 6.1 and 6.2.

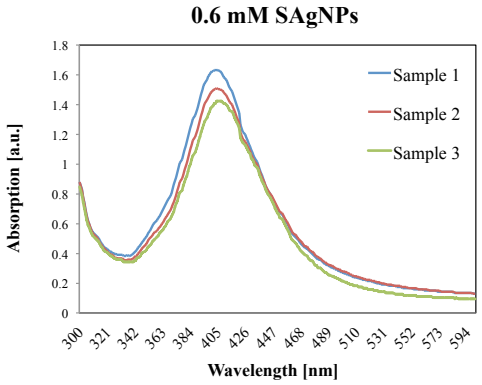

Figure 6.1. Three absorption spectra of SAgNPs in 0.6 mM concentrations. Absorption was measured, in a spectrophotometer, between 300 to 800 nm at an interval of 1 nm. The range has been adjusted to include only wavelengths from 300 to 600 nm.

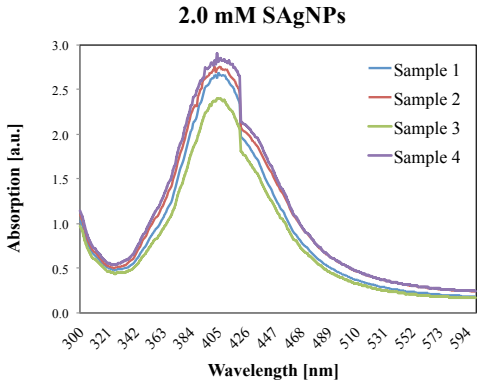

Figure 6.2. Four absorption spectra of SAgNPs in 2.0 mM concentrations. Absorption was measured, in a spectrophotometer, between 300 to 800 nm at an interval of 1 nm. The range has been adjusted to include only wavelengths from 300 to 600 nm.

For the concentration of 0.6 mM, three samples were tested as three solutions were made during the experiment. As can be seen from Figure 6.1 the 0.6 mM SAgNPs show λ_{max} at 404 nm in sample 1 and 2, while sample 3 shows λ_{max} at 406 nm. For the 2.0 mM SAgNPs, four samples were tested as four solutions were made during the experiment. As can be seen from Figure 6.2 the 2.0 mM SAgNPs show λ_{max} at 405 nm for sample 1, 402 nm for sample 2, 406 nm for sample 3, and 404 nm for sample 4.

For AFM measurement a drop of one solution of the 0.6 mM concentration was dropped on a mica plate and left to dry. Afterwards the mica plate was measured using AFM in dynamic mode yielding the picture shown in Figure 6.4. Afterwards a profile was established using the software WsxM 5.0 Develop 6.5 shown in Figure 6.3. The profile was created by measuring nine of the green dots from Figure 6.4. Figure 6.4 was modified using a different color scale, in order to make the nanoparticles easier to identify, indicated by the green dots.

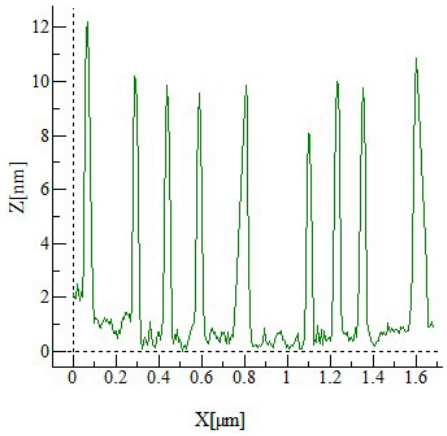

Figure 6.3. Profile of nine of the SAgNPs from Figure 6.4. The height of the SAgNPs vary from 8 to 12 nm. The software used was WsxM 5.0 Develop 6.5.

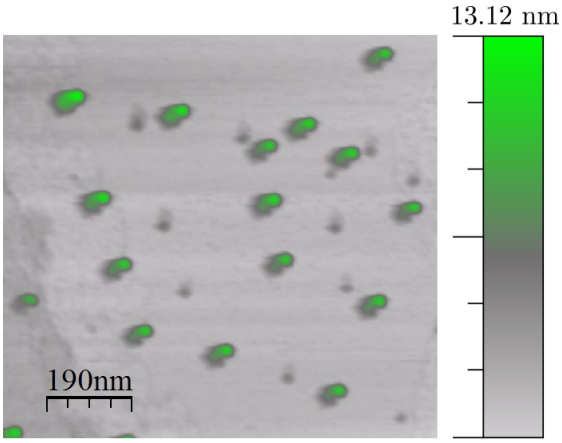

Figure 6.4. AFM measurement in dynamic mode of SAgNPs at 0.17 mM concentration on a mica plate. The colors were modified to enhance the contrast between the mica plate and the SAgNPs. The software used was WsxM 5.0 Develop 6.5.

The profile in Figure 6.3 shows that the height of the produced SAgNPs vary from 8 - 12 nm. Figure 6.4 shows 17 SAgNPs indicated by the green dots.

6.1.2 Triangular Silver Nanoprisms

After synthesis, 1 mL of the solution containing the assumed TAgNPs was tested by absorption spectroscopy yielding the absorption spectrum shown in Figure 6.5.

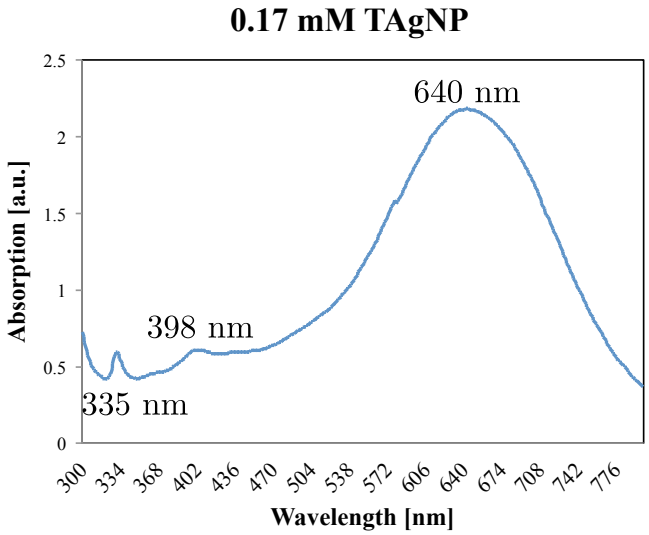

Figure 6.5. Absorption spectrum of 0.17 mM TAgNPs. Absorption was measured, in a spectrophotometer, between 300 - 800 nm with an interval of 1 nm.

The concentration of the TAgNPs was 0.17 mM. In figure 6.5, three peaks are observed. One at 335 nm, one at 398 nm, and one at 640 nm.
Furthermore, a picture was taken of the solutions containing TAgNPs, showing a deep blue color as can be seen in Figure 6.6.

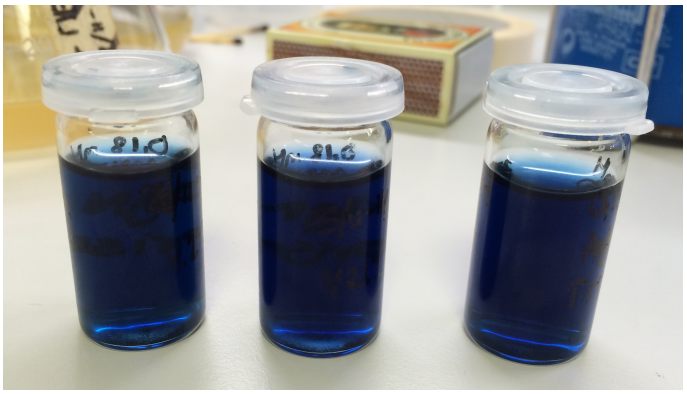

Figure 6.6. A picture showing the solutions containing TAgNPs just after the synthesis.

6.2 Standard Growth Curves

To determine the bactericidal effect of AgNPs, two standard growth curves were made, one for *E. coli* and one for *B. subtilis*. Each growth curve is an average between three individual growth curves made from three different precultures, where 2 mL of preculture was inoculated in 100 mL broth.

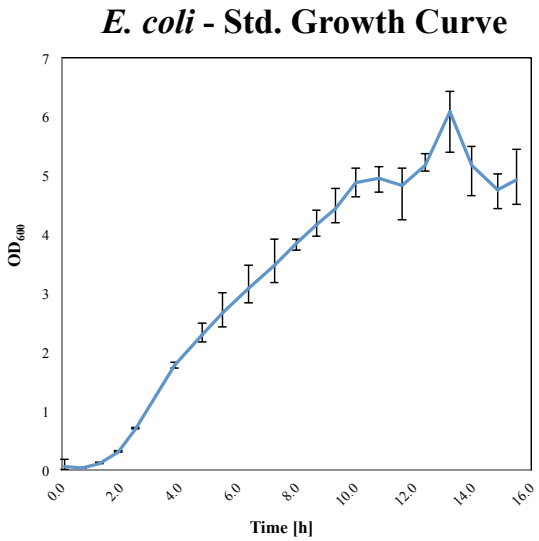

Figure 6.7. OD_{600} measurements taken with a spectrophotometer over 15 hours and 30 minutes with an interval of 30 - 60 minutes, giving an averaged standard growth curve of *E. coli* with no antimicrobial agents added to the LB broth. The cultures used were made from 2 mL preculture inoculated in 100 mL LB broth, stored in an incubator shaker at 37 °C at 230 rpm. The sample solutions measured were diluted before OD_{600} reached 0.7, 2.8, and 5.6, by a factor 4, 8, and 10 respectively.

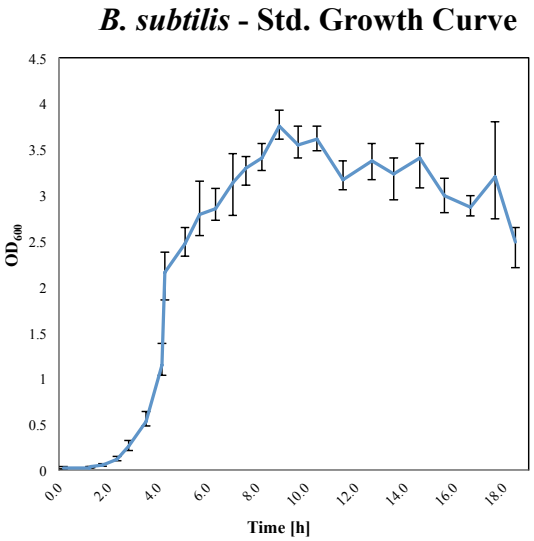

Figure 6.8. OD_{600} measurement taken with a spectrophotometer over 18 hours and 30 minutes with an interval of 30 - 60 minutes, giving an averaged standard growth curve of *B. subtilis* with no antimicrobial agents added to the YP broth. The cultures used were made from 2 mL preculture inoculated in 100 mL YP broth, stored in an incubator shaker at 37 °C at 230 rpm. The sample solutions measured were diluted before OD_{600} reached 0.7 and 2.8, by a factor 4 and 10 respectively.

To measure the OD_{600} accurately, the culture samples were diluted by a factor 4 before reaching 0.7 in absorbance and later diluted by a factor 8 before reaching 2.8 in absorbance. *E. coli* was furthermore diluted by a factor 10 before reaching 5.6 in absorption. The error bars on both curves show the spread between the three original growth curves from each experiment.

6.3 Bactericidal Effect of Silver Ions

The growth curves were determined from 1 mL of the culture solutions measured in a spectrophotometer at 600 nm at intervals of 30 - 60 minutes.

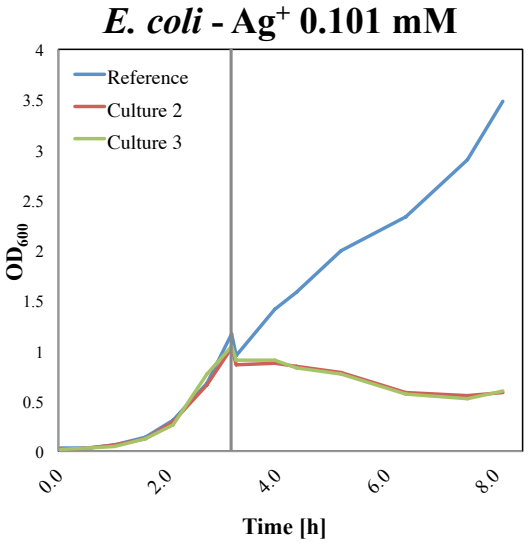

Figure 6.9. OD_{600} measurements taken with a spectrophotometer over 8 hours and 9 minutes with an interval of 30 - 60 minutes. The blue growth curve shows the reference culture of *E. coli*, where 15 mL 0.9 % NaCl solution was added at the same time as the silver ions in the other cultures. The green and red curves show cultures 2 and 3, where 15 mL of 0.74 mM silver ions were added 3 hours and 16 minutes after inoculation of the preculture. This resulted in a concentration of 0.103 mM silver ions in the broths. All three cultures were measured at the same time. All cultures were made by 1.5 mL of the same preculture inoculated in 100 mL LB broth. The vertical grey line shows the time of addition of both silver ions and NaCl solution. The sample solutions measured were diluted before OD_{600} reached 0.7 and 2.8, by a factor 4 and 8 respectively.

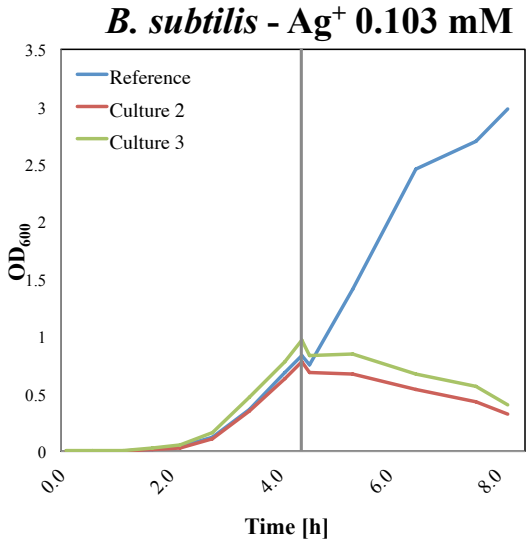

Figure 6.10. OD_{600} measurements taken with a spectrophotometer over 8 hours and 11 minutes with an interval of 30 - 60 minutes. The blue growth curve shows the reference culture of *B. subtilis*, where 15 mL 0.9 % NaCl solution was added at the same time as the silver ions in the other cultures. The green and red curves show cultures 2 and 3, where 15 mL of 0.74 mM silver ions were added 4 hours and 33 minutes after inoculation of the preculture. This resulted in a concentration of 0.103 mM silver ions in the broths. All three cultures were measured at the same time. All cultures were made by 1.5 mL of the same preculture inoculated in 100 mL YP broth. The vertical grey line shows the time of addition of both silver ions and NaCl solution. The sample solutions measured were diluted before OD_{600} reached 0.7 and 2.8, by a factor 4 and 8 respectively.

15 mL 0.74 mM silver ions were added to the cultures 2 and 3 and the physiological salt to the reference culture 3 hours and 16 minutes after the experiment was begun for *E. coli*, shown in Figure 6.9, and 4 hours and 33 minutes for *B. subtilis*, shown in Figure 6.10. This resulted in a silver concentration of 0.101 mM in the broth with *E. coli* and 0.103 mM in the broth with *B. subtilis*. The time is indicated by the grey vertical line present on both graphs. To measure the OD_{600} accurately, the culture samples were diluted by a factor 4 before reaching 0.7 in absorbance and later diluted by a factor 8 before reaching 2.8 in absorbance.

The growth curves were determined from 1 mL of the culture solutions measured in a spectrophotometer at 600 nm at intervals of 30 - 60 minutes.

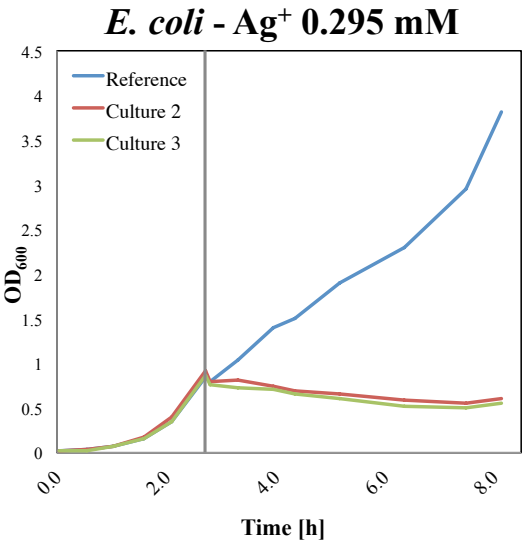

Figure 6.11. OD_{600} measurements taken with a spectrophotometer over 8 hours and 9 minutes with an interval of 30 - 60 minutes. The blue growth curve shows the reference culture of *E. coli*, where 15 mL 0.9 % NaCl solution was added at the same time as the silver ions in the other cultures. The green and red curves show cultures 2 and 3, where 15 mL of 2.16 mM silver ions were added 2 hours and 49 minutes after inoculation of the preculture. This resulted in a concentration of 0.295 mM silver ions in the broths. All three cultures were measured at the same time. All cultures were made by 1.5 mL of the same preculture inoculated in 100 mL LB broth. The vertical grey line shows the time of addition of both silver ions and NaCl solution. The sample solutions measured were diluted before OD_{600} reached 0.7 and 2.8, by a factor 4 and 8 respectively.

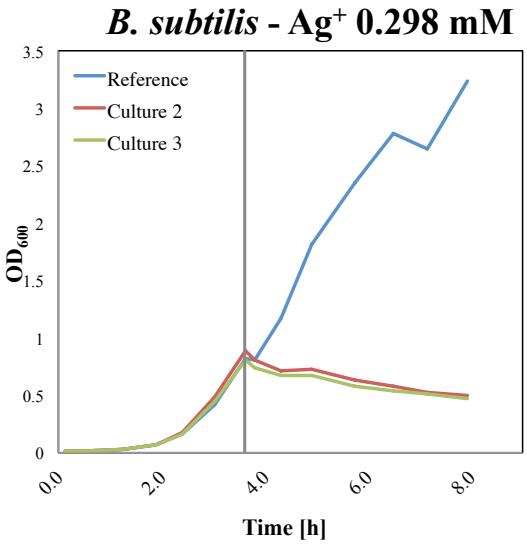

Figure 6.12. OD_{600} measurements taken with a spectrophotometer over 7 hours and 56 minutes with an interval of 30 - 60 minutes. The blue growth curve shows the reference culture of *B. subtilis*, where 15 mL 0.9 % NaCl solution was added at the same time as the silver ions in the other cultures. The green and red curves show cultures 2 and 3, where 15 mL of 2.16 mM silver ions were added 3 hours and 48 minutes after inoculation. This resulted in a concentration of 0.298 mM silver ions in the broths. All three cultures were measured at the same time. All cultures were made by 1.5 mL of the same preculture inoculated in 100 mL YP broth. The vertical grey line shows the time of addition of both silver ions and NaCl solution. The sample solutions measured were diluted before OD_{600} reached 0.7 and 2.8, by a factor 4 and 8 respectively.

15 mL 2.16 mM silver ions were added to the cultures 2 and 3 and the physiological salt to the reference culture 2 hours and 49 minutes after the experiment began for *E. coli*, shown in Figure 6.11, and 3 hours and 48 minutes for *B. subtilis*, shown in Figure 6.12. This resulted in a silver concentration of 0.295 mM in the broth with *E. coli* and 0.298 mM in the broth with *B. subtilis*. The time is indicated by the grey vertical line present on both graphs. To measure the OD_{600} accurately the culture samples were diluted by a factor 4 before reaching 0.7 in absorbance and later diluted by a factor 8 before reaching 2.8 in absorbance.

6.4 Bactericidal Effect of Spherical Silver Nanoparticles

The growth curves were determined from 1 mL of the culture solutions measured in a spectrophotometer at 600 nm at intervals of 30 - 60 minutes.

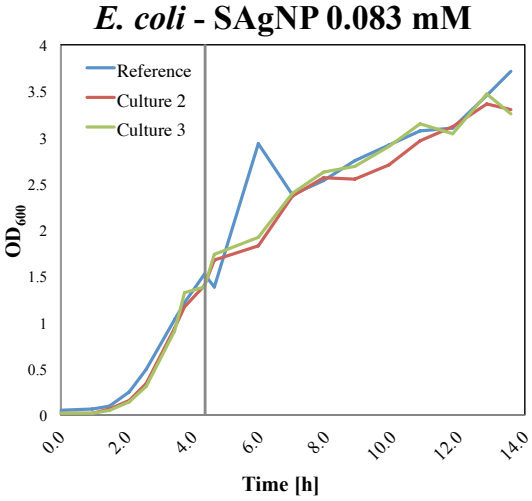

Figure 6.13. OD_{600} measurements taken with a spectrophotometer over 13 hours and 36 minutes with an interval of 30 - 60 minutes. The blue growth curve shows the reference culture of *E. coli*, where 15 mL 0.9 % NaCl solution was added at the same time as the SAgNPs in the other cultures. The green and red curves represent cultures 2 and 3, where 15 mL of 0.60 mM SAgNPs were added 4 hours and 39 minutes after inoculation of the preculture. This resulted in a concentration of 0.083 mM silver ions in the broths. All three cultures were measured at the same time. All cultures were made by 1.5 mL of the same preculture inoculated in 100 mL LB broth. The vertical grey line shows the time of addition of both SAgNPs and NaCl solution. The sample solutions measured were diluted before OD_{600} reached 0.7 and 2.8, by a factor 4 and 8 respectively.

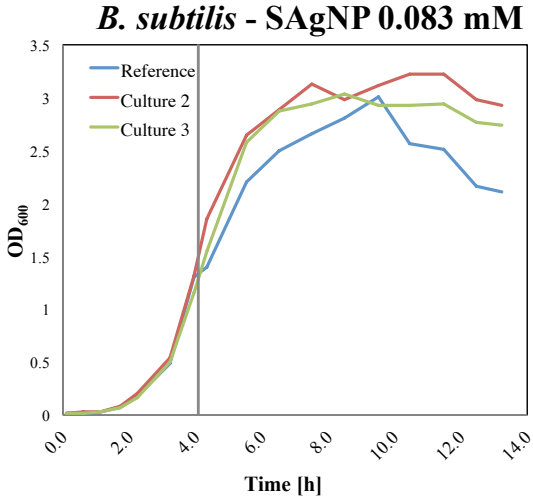

Figure 6.14. OD_{600} measurements taken with a spectrophotometer over 13 hours and 14 minutes with an interval of 30 - 60 minutes. The blue growth curve shows the reference culture of *B. subtilis*, where 15 mL 0.9 % NaCl solution was added at the same time as the SAgNPs in the other cultures. The green and red curves represent individual cultures where 15 mL of 0.60 mM SAgNPs were added 4 hours and 20 minutes after inoculation of the preculture. This resulted in a concentration of 0.083 mM silver ions in the broths. All three cultures were measured at the same time. All cultures were made by 1.5 mL of the same preculture inoculated in 100 mL YP broth. The vertical grey line shows the time of addition of both SAgNPs and NaCl solution. The sample solutions measured were diluted before OD_{600} reached 0.7 and 2.8, by a factor 4 and 8 respectively.

15 mL 0.60 mM SAgNPs were added to the cultures 2 and 3 and the physiological salt to the reference culture 4 hours and 39 minutes after the experiment was begun for *E. coli*, shown in Figure 6.13, and 4 hours and 20 minutes for *B. subtilis*, shown in Figure 6.14. This resulted in a silver concentration of 0.083 mM in the broth with *E. coli* and 0.083 mM in the broth with *B. subtilis*. The time is indicated by the grey vertical line present om both graphs. To measure the OD_{600} accurately the culture samples were diluted by a factor 4 before reaching 0.7 in absorbance and later diluted by a factor 8 before reaching 2.8 in absorbance.

The growth curves were determined from 1 mL of the culture solutions measured in a spectrophotometer at 600 nm at intervals of 30 - 60 minutes.

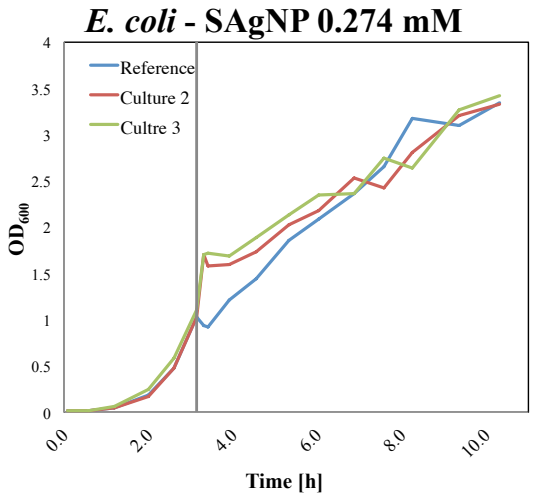

Figure 6.15. OD_{600} measurements taken with a spectrophotometer over 10 hours and 19 minutes with an interval of 30 - 60 minutes. The blue growth curve shows the reference culture of *E. coli*, where 15 mL 0.9 % NaCl solution was added at the same time as the SAgNPs in the other cultures. The green and red curves show cultures 2 and 3 where 15 mL of 2.00 mM SAgNPs were added 3 hours and 18 minutes after inoculation of the preculture. This resulted in a concentration of 0.274 mM silver ions in the broths. All three cultures were measured at the same time. All cultures were made by 1.5 mL of the same preculture inoculated in 100 mL LB broth. The vertical grey line shows the time of addition of both SAgNPs and NaCl solution. The sample solutions measured were diluted before OD_{600} reached 0.7 and 2.8, by a factor 4 and 8 respectively.

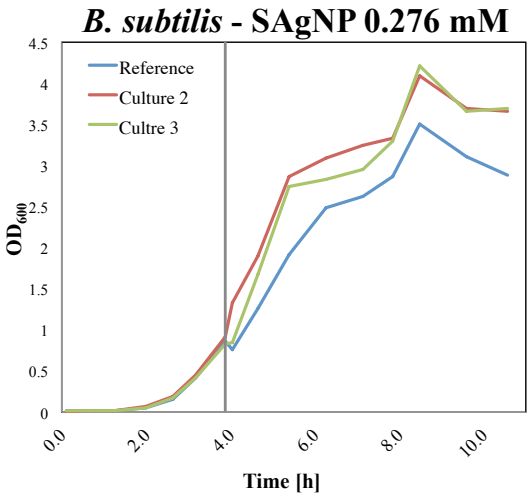

Figure 6.16. OD_{600} measurements taken with a spectrophotometer over 10 hours and 34 minutes with an interval of 30 - 60 minutes. The blue growth curve shows the reference culture of *B. subtilis*, where 15 mL 0.9 % NaCl solution was added at the same time as the SAgNPs in the other cultures. The green and red curves show cultures 2 and 3 where 15 mL of 2.00 mM SAgNPs were added 4 hours and 3 minutes after inoculation of the preculture. This resulted in a concentration of 0.276 mM silver ions in the broths. All three cultures were measured at the same time. All cultures were made by 1.5 mL of the same preculture inoculated in 100 mL YP broth. The vertical grey line shows the time of addition of both SAgNPs and NaCl solution. The sample solutions measured were diluted before OD_{600} reached 0.7 and 2.8, by a factor 4 and 8 respectively.

15 mL 2.00 mM SAgNPs were added to the cultures 2 and 3 and the physiological salt to the reference culture 3 hours and 18 minutes after the experiment was begun for *E. coli*, shown in Figure 6.15, and 4 hours and 3 minutes for *B. subtilis*, shown in Figure 6.16. This resulted in a silver concentration of 0.274 mM in the broth with *E. coli* and 0.276 mM in the broth with *B. subtilis*. The time is indicated by the grey vertical line present on both graphs. To measure the OD_{600} accurately the culture samples were diluted by a factor 4 before reaching 0.7 in absorbance and later diluted by a factor 8 before reaching 2.8 in absorbance.

6.5 Bactericidal Effect of Triangular Silver Nanoprisms

The growth curves were determined from 1 mL of the culture solutions measured in a spectrophotometer at 600 nm at intervals of 30 - 60 minutes.

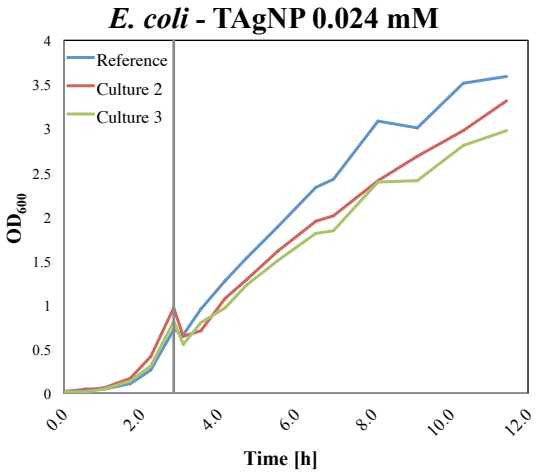

Figure 6.17. OD_{600} measurements taken with a spectrophotometer over 11 hours and 27 minutes with an interval of 30 - 60 minutes. The blue growth curve shows the reference culture of *E. coli*, where 15 mL 0.9 % NaCl solution was added at the same time as the TAgNPs in the other cultures. The green and red curves show cultures 2 and 3 where 15 mL of 0.17 mM silver nanoprisms were added 3 hours and 5 minutes after inoculation of the preculture. This resulted in a concentration of 0.024 mM silver ions in the broths. All three cultures were measured at the same time. All cultures were made by 1.5 mL of the same preculture inoculated in 100 mL LB broth. The vertical grey line shows the time of addition of both TAgNPs and NaCl solution. The sample solutions measured were diluted before OD_{600} reached 0.7 and 2.8, by a factor 4 and 8 respectively.

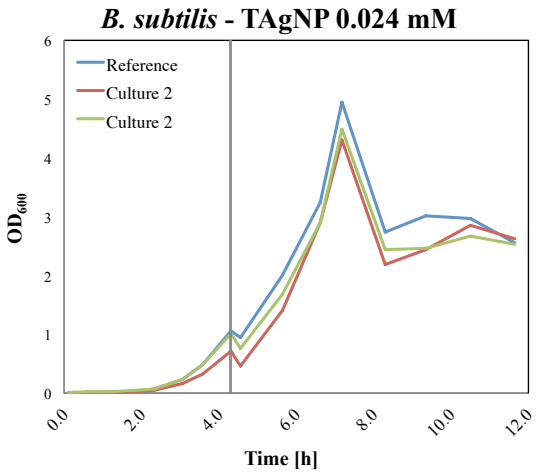

Figure 6.18. OD_{600} measurements taken with a spectrophotometer over 11 hours and 39 minutes with an interval of 30 - 60 minutes. The blue growth curve shows the reference culture of *B. subtilis*, where 15 mL 0.9 % NaCl solution was added at the same time as the TAgNPs in the other cultures. The green and red curves show cultures 2 and 3 where 15 mL of 0.17 mM silver nanoprisms were added 4 hours and 34 minutes after inoculation of the preculture. This resulted in a concentration of 0.024 mM silver ions in the broths. All three cultures were measured at the same time. All cultures were made by 1.5 mL of the same preculture inoculated in 100 mL YP broth. The vertical grey line shows the time of addition of both TAgNPs and NaCl solution. The sample solutions measured were diluted before OD_{600} reached 0.7 and 2.8, by a factor 4 and 8 respectively.

15 mL 0.17 mM TAgNPs were added to the cultures 2 and 3 and the physiological salt to the reference culture 3 hours and 5 minutes after the experiment was begun for *E. coli*, shown in Figure 6.17, and 4 hours and 34 minutes for *B. subtilis*, shown in Figure 6.18. This resulted in a silver concentration of 0.024 mM in the broth with *E. coli* and 0.024 mM in the broth with *B. subtilis*. The time is indicated by the grey vertical line present on both graphs. To measure the OD_{600} accurately the culture samples were diluted by a factor 4 before reaching 0.7 in absorbance and later diluted by a factor 8 before reaching 2.8 in absorbance.

7. Discussion

7.1 Characterisation of the Silver Nanoparticles

The absorption spectra of both the SAgNPs and TAgNPs reveal information about their shape. The SAgNPs will show a peak in absorption at the wavelength corresponding to the plasmon resonance frequency for spherical nanoparticles. This makes it possible to predict where the peak in absorption will occur, and it is then possible to determine the shape of the SAgNPs from their absorption spectrum.
The TAgNPs had a different absorption spectrum due to their shape, and the calculations allowing one to predict the maximum absorption wavelength are much more complicated and beyond the scope of this project. The absorption spectrum of the TAgNPs will therefore be discussed in relation to the current research, and the observations other reports have made in relation to it.

7.1.1 Spherical Silver Nanoparticles

As shown in Section 4.1, the wavelength corresponding to the plasmon resonance frequency could be determined by absorption spectroscopy, as there would be a peak in absorption around this wavelength. The measured absorption spectrum of the SAgNPs can be seen in Figures 6.1 and 6.2, and the maximum absorption wavelengths can be seen in Table 7.1.

Sample number	λ_{max} **in 0.6 mM**	λ_{max} **in 2.0 mM**
Theory	397.33 nm	397.33 nm
1	404 nm	404 nm
2	404 nm	402 nm
3	406 nm	406 nm
4	•	404 nm

Table 7.1. λ_{max} for both 0.6 mM and 2.0 mM concentrations of SAgNPs. λ_{max} is approximately 8 - 10 nm from the theoretical value obtained in Subsection 4.1.5, which was at 397.33 nm.

In Subsection 4.1.5, the maximum absorption wavelength was predicted to be approximately 397.33 nm. As can be seen from Table 7.1, the experimental maximum absorption wavelengths were all slightly displaced in the spectrum having a λ_{max} value 8 - 10 nm greater than the theoretical maximum absorption wavelength. This difference can be attributed to the fact that the particles are suspended in broths, which can lead to some formation of silver ions. When nanoparticles, which have a much larger surface-to-volume ratio, are suspended, in relation to bulk silver, more ions can be produced. However, this displacement is considered small, making it highly likely that there was indeed synthesized SAgNPs. These λ_{max} values are similar to the current research [10, 48, 51, 84, 85, 86] as is evident from the graphs in Figures 7.1 and 7.2.

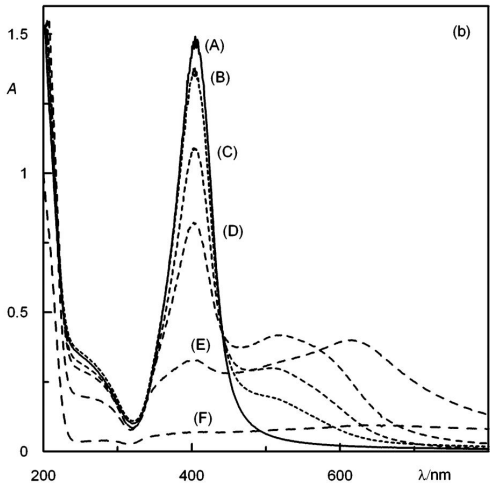

Figure 7.1. Maximum absorption wavelength of SAgNPs showing the destabilizing ability of poly(diallyldimethylammonium) chloride (PDDA) solutions. The information relevant for this report is sample (A) as it contains no PDDA solution. The graph is obtained from Kvitek *et al.* showing the maximum absorption wavelength at approximately 400 nm. [51]

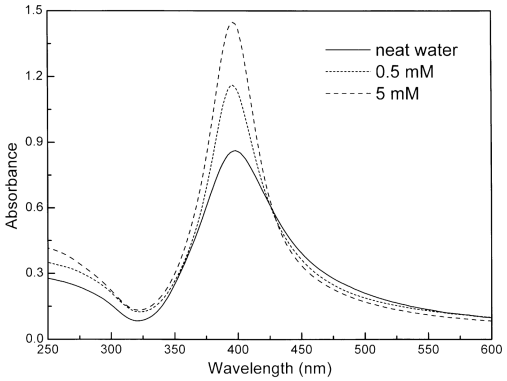

Figure 7.2. Maximum absorption wavelength of SAgNPs at different concentrations of sodium chloride obtained from Bae *et al.* showing the maximum absorption wavelength at approximately 400 nm [86].

Another point of interest is to investigate the width of the peak at half height, the full-width half-maximum (FWHM) of the experimental and theoretical graphs and compare them with other research, as seen in Table 7.2.

Source	**Size of SAgNPs**	$\lambda_{\mathbf{max}}$	**FWHM**
Theory	N/A	397.33 nm	40 nm
Experimental	8 - 12 nm	402 - 406 nm	75 - 85 nm
Mulfinger *et al.* [48]	10 - 14 nm	395 - 405 nm	50 - 70 nm
Bae *et al.* [86]	25 - 30 nm	400 nm	75 nm
Kamat *et al.* [87]	35 - 50 nm	420 nm	100 - 110 nm
Nair *et al.* [88]	60 - 80 nm	438 nm	140 - 150 nm

Table 7.2. The table shows FWHM from both the theory in Section 4.1 and the experiments done together with the values from the current research. The table is ordered by sizes of the SAgNPs. Note that the size derived from theory is non-applicable as $\lambda_{\max}$ does not depend on the diameter of the SAgNPs in the theory used in this project.

The experimental FWHM from this project is twice the size of the theoretical FWHM, which according to Quentin *et al.* can be caused by a greater dielectric constant in the actual nanoparticles than the dielectric constants found by the database used in Section 4.1 [41]. The red-shift observed in particles between 35 - 50 nm and 60 - 80 nm in diameter may be caused by the size of the particles. The theory used in Section 4.1 assumes the size of the nanoparticles to be much less than that of the wavelength of the electromagnetic wave. At 60 - 80 nm the nanoparticle is almost one fifth the size of the wavelength, and the assumption that the E-field from the electromagnetic wave is homogenous around the particle might no longer be applicable.
Even though the shape of the SAgNPs becomes apparent from absorption spectroscopy,

their size does not, as a changed size of the SAgNPs would not change the maximum absorption wavelength. Therefore, AFM was used to measure the size of the SAgNPs, as can be seen in Figures 6.3 and 6.4. The measurements showed that the SAgNPs had a diameter between 8 - 12 nm. This size of SAgNPs conforms with the literature, where reports have made SAgNPs around the same size using different methods of synthesis [10, 48, 75, 76, 77, 84, 85]. These different methods of synthesis have been expanded on in Chapter 2. SAgNPs with this size should be very effective against bacteria [10, 51, 75, 77, 84], and the efficacy of the SAgNPs made in this project will be commented on in Section 7.2.
As stated in Section 4.3, the stabilizing agent, Tween 80, was needed to keep the SAgNPs from aggregating. Tween 80 is a non-ionic, non-toxic, and biocompatible surfactant [89], and it was chosen primarily due to the small effect it has on the bactericidal effect of the SAgNPs and the excellent stabilization it facilitates [51, 90]. Tween 80 stabilizes the SAgNPs by steric hindrance, meaning the molecules are adsorbed to the surface of the nanoparticles, thereby hindering any interactions between the SAgNPs, ideally resulting in no aggregation. When compared to larger surfactants, Tween 80 is adsorbed to the surface of the SAgNPs in a smaller, more compact way, which can be part of the reason behind the small disturbance in the bactericidal effects of the SAgNPs. [51]

7.1.2 Triangular Silver Nanoprisms

TAgNPs were synthesized as described in Section 4.4. As with SAgNPs, they were characterized using both absorption spectroscopy and AFM measurements. The spectroscopy measurements revealed a spectrum very much alike what is measured in current research [46, 47, 54, 91], see Figure 6.5. A visual inspection revealed a deep blue color of the nanoparticles, as shown in Figure 6.6, and this corresponds very well with a maximum absorption wavelength at 640 nm according to Kelly *et al.* [54]. Furthermore, the blue color could mean less truncated prisms, as mentioned in Section 4.2, which also corresponds to a λ_{max} value around 640 nm [45]. The AFM measurement done on the TAgNPs was not a success however, which is speculated to be related to the stabilizing agent, trisodium citrate. As mentioned in Section 4.4, trisodium citrate stabilizes by having negatively charged carboxylate groups pointing outwards, making the particle, as a whole, negatively charged. As described in Section 5.4, a mica plate was used during AFM measurements, and it is well known, that a mica surface is negatively charged [92]. This results in electrostatic repulsion between the particles and the mica surface, and if AFM measurements were to be made, a different stabilizer, such as Tween 80, should be used. It is however evident from both absorption spectroscopy and visual inspection that TAgNPs were indeed synthesized, even if their corresponding morphology could not be determined with AFM.

7.2 Bactericidal Effect toward *Escherichia coli* and *Bacillus subtilis*

In order to determine a bactericidal effect of AgNPs and silver ions, *E. coli* and *B. subtilis* were presented with optimal growth conditions. They were both incubated at 37 °C and aerobic conditions, which resulted in excellent growth of both bacteria. *E. coli* was cultivated in LB broth, whereas *B. subtilis* was cultivated in YP broth, since sodium chloride potentially can decrease the growth rate of *B. subtilis* according to Mercedes *et al.* [34].
For every experiment containing three cultures with one being a reference, 1.5 mL preculture was inoculated in each of the three cultures. This was done, to ensure that every culture had the same initial concentration of bacteria and potential impurities. When comparing OD_{600} in the beginning of the experiments, there was a negligible difference between the start concentrations which ranged from 0.013 to 0.016 in absorbance.
In every experiment, 15 mL of AgNP solutions were added to culture 2 and 3, while 15 mL of physiological salt (0.9 % sodium chloride) was added to the reference culture (culture 1). Physiological salt was added to the reference culture in the same volume as AgNP to culture 2 and 3 to present identical dilution factors. Right after addition, OD_{600} showed a drop in absorbance in most cultures. This is speculated to originate from dilution of the cultures and not the bactericidal effect of the AgNPs since the same drop occurred in the reference culture. The volume of the cultures were around 92 mL when the 15 mL AgNP solution was added giving a dilution factor of approximately 1.2, which is enough to show a decrease in absorbance.
Furthermore, the *E. coli* and *B. subtilis* cultures containing the lowest concentration of SAgNPs (0.083 mM in the broth) showed no drop in absorbance after addition of SAgNPs. This can be a result of a lack of correction being made, unlike every other experiment. An addition of 15 mL physiological salt to the *B. subtilis* reference cultures can potentially have decreased growth rate of the bacterium for a period of time. However, according to Mercedes *et al. B. subtilis* is excellent at adapting to changes in osmotic pressure [34], and it is evident that *B. subtilis* continued growth after the addition of the physiological salt.
A standard growth curves of both *B. subtilis* and *E. coli* was developed through 16 - 18 hours of OD_{600} measurements under optimal growth conditions for the bacteria in order to determine a point in growth when silver ions, SAgNPs and TAgNPs should be added. In this project, bactericidal agents were added during the third, fourth or the fifth growth hour (exponential phase) corresponding to OD_{600} ranging from 0.7 to 1.1 in absorbance.

7.2.1 Silver Ions

It is well known that silver ions have a high bactericidal effect toward both gram-negative and gram-positive bacteria, see Subsection 4.5. Silver ions are postulated to interact with enzymes participating in cell respiration, react with proteins crucial for membrane gradients such as PMF, and disturb cell electron density, only to mention a few antimicrobial effects of silver ions. It is evident from the experiments, described in Subsection 6.3, that both silver ion concentrations of 0.10 mM and 0.29 mM in the broths caused great bactericidal effects toward *E. coli* and *B. subtilis* immediately after addition.
This effect was expected, as silver ions have been used as an antimicrobial agent for cen-

turies, as mentioned in Section 1.1 [7]. The growth rate in both bacteria decreases, and one can argue, that in the case of *E. coli* some silver ions have reacted with chloride in the medium in order to form silver chloride. However, no difference in bactericidal effect toward *E. coli* and *B. subtilis* was observed. The concentration of silver ions in the cultures has been effective against the bacterial cell concentration at the time of addition.
Factors such as *B. subtilis* being significantly larger than *E. coli* resulting in a higher number of *E. coli* than *B subtilis* at similar OD_{600}, an equal concentration of silver were added to both bacteria, an equal bactericidal effect was observed in both of the experiments, and the OD_{600} measures total cell density, all point towards the fact, that silver ions might be more effective against *E. coli*. Feng *et al.* found similar results, when they demonstrated that silver ions are more effective against *E. coli* than the gram-positive bacterium *Staphylococcus aureus* (*S. aureus*). They speculate, that the thicker cell wall in gram-positive bacteria makes for a stronger defence against the silver ions [65]. The effect can also be explained by the fact that silver ions are more reactive toward components of the gram-negative outer cell membrane and thinner cell wall compared to the thicker cell wall of the gram-positive *B. subtilis*. Another explanation could be, that since *B. subtilis* bacteria are much larger than *E. coli*, it requires a higher concentration of silver ions to inhibit cell growth leading to lysis, and that *B. subtilis* might simply be more resistant against silver ions compared to *E. coli*.

7.2.2 Silver Nanoparticles

The bactericidal effects of both SAgNPs and TAgNPs have been examined, and the experiments revealed no bactericidal effect.
This can primarily be explained by the time of silver addition. The AgNPs were added in the third, fourth or fifth growth hour where the cell concentration of *E. coli* was between $5.6 \cdot 10^8$ to $8 \cdot 10^8$ cells per mL and for *B. subtilis* it was between $7 \cdot 10^7$ to $1.2 \cdot 10^8$ cells per mL [76]. The concentrations of silver in the culture broths in SAgNPs were 0.083 mM and 0.276 mM, and in TAgNPs it was 0.024 mM. The high concentration of bacterial cells and rather large volume of the cultures, compared to the rather low silver concentration, is probably the main reason for no observed bactericidal effect [76]. This is supported by the current research, which uses concentrations of silver in AgNPs against *E. coli* shown in Table 7.3. These concentrations are rather low. They are based on OD_{600} in broths, where AgNPs are present in the cultures at the moment of inoculation with *E. coli*, supporting that the times of addition used in the experiments in this project were too late. Moreover, Sondi *et al.* found that even at high concentrations in broth, SAgNPs caused only a delay in growth. They argue that, compared to solid media, the concentration of AgNPs decreases as the particles interact with cellular components. SEM pictures indicated macroscopic aggregations consisting of AgNPs and dead bacterial cells. Sondi *et al.* conclude that AgNPs have a limited use in liquid systems due to their low colloidal stability [76]. One could argue that, in these experiments, not only was the cell concentration too high and the concentration of silver too low, but particles acting as bactericidal agents aggregated together with dead cells, and would thereby be of no further use, and cells not affected would continue duplicating. Since OD_{600} measures total bio density, the aggregates will contribute to an increase in OD_{600} in the exponential phase, and the AgNPs will appear

to have no bactericidal effect.

Reference	Diameter	Concentration
Shrivastava *et al.* [78]	10 - 15 nm	0.23 mM
Sondi *et al.* [76]	10 - 16 nm	0.46 mM
Raffi *et al.* [75]	16 nm	0.56 mM
Pal *et al.* [84]	39 nm	0.46 mM

Table 7.3. The smallest concentrations of SAgNPs with different diameters having a considerable effect on bacterial growth being used against *E. coli* in broth, in the current research.

The experiments in this project does not conclude, that the AgNPs have no bactericidal effects. According to Sondi *et al.*, one can argue that the cell concentrations in the experiments are higher than what can be found in any real-life system. If the bactericidal effects of AgNPs are to be evaluated, the particles should be present when the media is inoculated. This is the preferred method of the current research, and it is more akin to real life situations. [6, 8, 10, 75, 76, 84]
It is suggested that the release of ions is the only, or primary, reason for bactericidal effect of nanoparticles, and that AgNPs offers a slow and controlled release of silver ions compared to reactive silver salts [58, 59]. The reactivity of silver ions toward *E. coli* and *B. subtilis* are well demonstrated, and this effect did not occur at all in the experiments with both SAgNPs and TAgNPs. However, it is difficult to determine whether any silver ions were dissolved from the AgNPs at all. No bactericidal effect of the AgNPs was observed, but since the particle concentration was low compared to the cell concentration, the ion concentration would be even lower and its effect would not be detectable in the high cell concentration. Furthermore, if the AgNPs should release silver ions, one could argue that the TAgNPs would release more ions due to their higher surface-to-volume ratio and higher percentage of the atom dence {111} facets, and would, compared to SAgNPs in same concentration, have a higher bactericidal effect. One should note, it is the concentration of silver atoms that is mentioned throughout the project and not the concentration of AgNPs. Less atoms make up the surface of a spherical particle than a triangular particle of the same volume. More atoms are on the surface of the triangular particles making them more reactive. This means that it is difficult to compare the experiments on bactericidal effect of TAgNPs, SAgNPs, and silver ions toward *E. coli* and *B. subtilis*, since the number of particles in the TAgNP solution is lesser than in the SAgNP solution, and both are significantly lower than the number of free ions in the silver ion solution, even though the atom concentration is the same.
Furthermore, it is evident that, for AgNPs to release silver ions, there must be a highly oxidizing environment, see Section 4.5.1. The intracellular environment is slightly oxidative, and the particle solutions are highly reductive due to sodium borohydride. Peroxides can represent an oxidizing environment, but intracellularly there is a negligible concentration of peroxides and other oxidizing agents, primarily due to specialized enzymes that deal with the cytotoxic oxygen species. One could argue that, AgNPs potentially can comprehensively inhibit these enzymes resulting in an increase in ROS, that afterwards can oxidize silver ions from the AgNPs. The release of ions is further demonstrated to depend on pH by Liu *et al.*, where pH 7 resulted in release of small concentrations of silver ions from AgNPs in the presence of free protons. One could argue that, when inside the

periplasmic space, free protons are available due to the PMF, allowing AgNPs to release silver ions during reaction with dissolved oxygen. In the experiments in this project, there could be only a very small concentration of free silver ions, since there is no oxidative environment either in the media or intracellularly. The pH is 7 both in the culture and intracellularly, and there is no acidic environment providing protons to begin with. Acidic and oxidizing environments might occur when the AgNP interact with the cell membrane, the cell wall, and their components during accumulation, and further by gab formation, thus entering the cell. Smaller particles might just diffuse over the cell membrane like water and other small molecules. Morones *et al.* demonstrated that AgNPs suspended in 0.2 M sodium nitrate released silver ions at concentrations of < 1 μM. In their experiment, there was 287 times more sodium nitrate present than silver. In this project, however, there was an equal concentration of sodium nitrate and silver present after the synthesis of SAgNPs, and thus the formation of ions caused by sodium nitrate will be negligible. [56]
A way of combatting the problem of too low particle concentration is to increase the concentration by other synthesis methods. A synthesis method proposed by Pastoriza-Santos *et al.* should make it possible to increase the silver nitrate stock concentration 20 times compared to the concentration used in the experiment with TAgNPs [93]. Increasing the concentration would not solve all problems, since the amount of particles still would be very small compared to the number of bacterial cells, and other reports are able to observe bactericidal effects when concentrations similar to those in this project are used [84]. The final solution should therefore be, as mentioned, to add the particles during inoculation of bacteria.
The stabilizer used in the synthesis of the TAgNPs was trisodium citrate, which as explained in Section 4.4, establishes a negatively charged electrostatic hindrance between the nanoparticles. This could give problems when investigating the bactericidal effect, as bacterial cell membranes are negatively charged due to the phosphoric-acid group in phospholipids. If the surface of either *B. subtilis* or *E. coli* is negatively charged, the TAgNPs would be repulsed by electrostatic forces, and no direct cell damage would be possible. With no direct cell contact, no accumulation onto cell envelope, no interaction with enzymes and proteins, no entering the cell, and no change in the intracellular environment releasing silver ions is possible. A solution would have been to use Tween 80 as a stabilizing agent instead, while synthesizing TAgNPs.
Even though AgNPs are proven to have great antimicrobial effects toward a wide range of microorganisms [9, 10], one must especially consider nanotoxicity when applying AgNPs in infectious treatments and other bacterial growth controls. More profound studies in the field of nanotoxicity is needed before one should apply AgNPs at higher industrial levels to prevent unexpected societal health problems, primarily due to discharge into the valuable aqueous ecosystems. Furthermore, it is suggested that silver nanoparticles cannot discriminate between different strains of bacteria and can hence lead to cell death in microbes beneficial to the environment [9]. The central nervous system is especially vulnerable to direct exposure of AgNPs resulting in primarily oxidative stress and inflammation, and a potential development of Alzheimers and Parkinsons. [94]
Moreover, AgNPs are popular in bandages to prevent bacterial inflammation. However, it is not *E. coli* and *B. subtilis* one will primarily find in skin infections, but other bacteria such as *S. aureus*.
S. aureus is almost always responsible for infections of the skin and wounds [2], and

so if AgNPs are to be used in bandages and the like, there is need for study of this bacterium. It is a gram-positive bacterium, which means it has a cell envelope similar to that of *B. subtilis*. Extensive research has gone into exploring what bactericidal effect, AgNPs have on *S. aureus*, and many studies have had somewhat successful experiments [78, 95, 96, 97, 98]. According to Shrivastava *et al.*, it is evident that AgNPs is not as successful against *S. aureus* as it is the case with *E. coli*. Copper has also been investigated as an efficient bactericidal agent against *S. aureus*, but Ruparelia *et al.* found that silver was approximately 10 - 15 % more effective against *S. aureus* than copper [97]. Li *et al.* found that a concentration of 0.19 mM AgNPs had a considerable bactericidal effect on *S. aureus* in broths. [98]

7.3 Other Experimental Considerations

In this project, OD_{600} was used for measuring the bactericidal effects of AgNPs. It is a very useful method used by many, and if the AgNPs in this project were added at the time of inoculation, results like Raffi *et al.* as seen in Figure 7.3 could be obtained [75]. Their results clearly shows the bactericidal effect AgNPs can have on *E. coli* in broth.

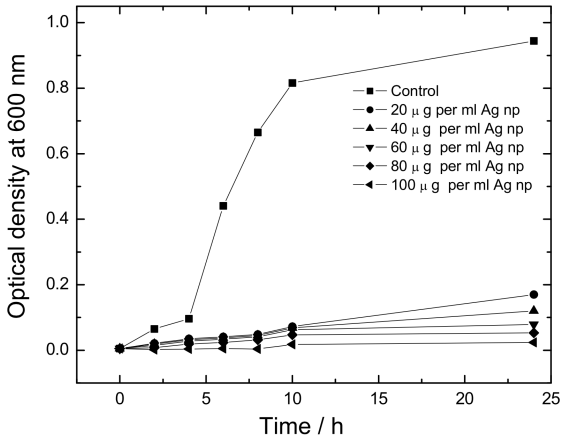

Figure 7.3. OD_{600} measurements showing minimal growth when *E. coli* is exposed to AgNPs [75].

A method more suitable for a quantitative comparison between different kinds of AgNPs could be measuring the minimum inhibitory concentration (MIC) and the minimal lethal concentration (MLC) [76, 99]. The MIC is the lowest concentration that will inhibit the visible growth of a microorganism during overnight incubation on agar plates, and MLC is the minimum concentration that will kill 99 % of the bacteria during overnight incubation on agar plates. When measuring the MIC and MLC of AgNPs, agar plates with different concentrations of particles and a constant number of colony-forming units (CFU) of a bacteria is incubated over night in 37 °C. The formed colonies are counted, and either the MLC or MIC is evaluated. Figure 7.4 provides an experiment done by Raffi *et al.*. [75]

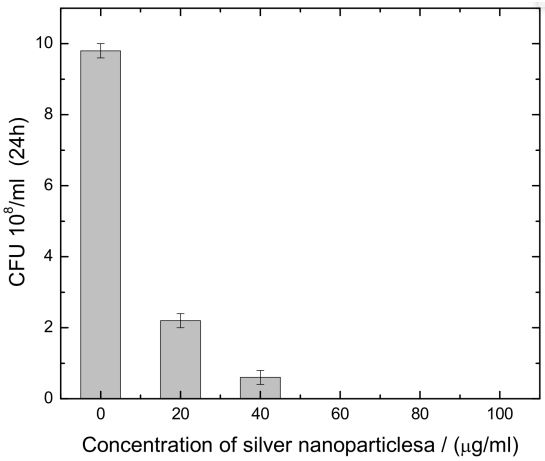

Figure 7.4. A measurement of the number of CFU of *E. coli* on agar plates after overnight incubation with different concentrations of AgNPs [75].

One way to do a MLC measurement is to incubate an agar plate overnight, and then place

a small volume of nanoparticles in the middle of the plate. The plate is then incubated overnight once more, and the bactericidal effect of the particles should be visible. The effect is seen as an inhibition zone containing no or very few CFU. The inhibition zone varies in size as a function of both volume and concentration of the added particles. Methods measuring MLC and MIC has a distinct advantage over methods relying on OD_{600}, since the results are more easily quantifiable and it is easier to compare different kinds of nanoparticles. Furthermore, methods observing MIC and MLC escapes some of the disadvantages of OD measurements such as dead bacterial cells being counted as metabolically active ones. OD_{600} is a very popular method, which makes it possible to observe the growth of the bacteria easily, and a usage of both methods must be recommended for a full analysis.

As described in Subsection 4.5.4 the shape of the nanoparticles is widely accepted to greatly influence the antimicrobial effect of silver nanoparticles. A larger surface-to-volume ratio results in a greater bactericidal effect and so, another shape could have been tried in this project. One shape in particular, the tetrahedron, has the largest surface-to-volume ratio and methods already exist to synthesize these, like the one used by Wiley *et al.* [100]. Single-crystal cubes and tetrahedrons of silver nanoparticles with truncated corners are synthesized by reducing silver nitrate with ethylene glycol while heating it to 148 °C, and using poly(vinyl purrolidone) as a stabilizing agent. By varying the synthesis time, Wiley *et al.* was able to make silver nanoparticles in the range of 20 to 80 nm [100].

Different metals and materials will have different bactericidal properties. Especially interesting, apart from silver, is copper, zinc, titanuim, magnesium and gold. According to Rai *et al.* silver is proven to be the most effective bactericidal agent against microorganisms, but copper has also been investigated [7, 97, 101]. A distinction, when investigating bactericidal effects, must be made between the gram-positive bacteria and the gram-negative. According to Ruparelia *et al.*, copper nanoparticles is found to be more effective when treating *B. subtilis* than AgNPs. This can be seen in Figure 7.5. [97]

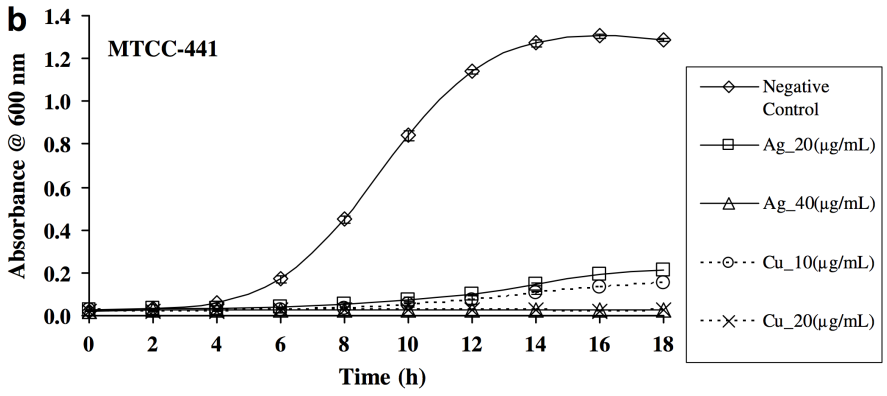

Figure 7.5. OD_{600} measurements showing that copper nanoparticles is more effective in impairing growth of *B. subtilis* than AgNPs [97].

This is speculated to be because of the large number of amines and carboxylic groups in the cell wall of the gram-positive bacteria, and the high affinity towards reactions with them in copper nanoparticles [97, 101]. A reason behind the need for other antimicrobial agents besides AgNPs is the risk for a development of drug resistance in some bacterial strains [8].

8. Conclusion

The objective of this project was to determine the bactericidal effect of SAgNPs, TAgNPs, and silver ions, and to see if the cell envelope difference between gram-positive (*B. subtilis*) and gram-negative (*E. coli*) bacteria makes any difference in the bactericidal effect. This was done by cultivating *B. subtilis* and *E. coli* in YP broth and LB broth respectively, then adding either silver ions, SAgNPs, or TAgNPs to the cultures at a specific OD_{600} value. To ensure that it was indeed SAgNPs and TAgNPs, that was added to the cultures, the AgNPs were characterized through absorption spectroscopy and AFM measurements, although the AFM measurement did not succeed with TAgNPs, most likely because of the stabilizer used in the synthesis. The SAgNPs were found to be between 8 and 12 nm in diameter. A standard growth curve for both *E. coli* and *B. subtilis* was made to determine when the antimicrobial agents should be added. It was decided to add the antimicrobial agents between OD_{600} values of 0.7 and 1.1. Five experiments were conducted for each bacteria. For *E. coli*; SAgNPs at 0.083 mM and 0.274 mM, TAgNPs at 0.024 mM, and silver ions at 0.101 mM and 0.295 mM. For *B. subtilis*; SAgNPs at 0.083 mM and 0.276 mM, TAgNPs at 0.024 mM, and silver ions at 0.103 mM and 0.298 mM. All concentrations are of silver in the culture broths. All experiments with silver ions showed a bactericidal effect, while every experiment with TAgNPs and SAgNPs showed no bactericidal effect. This was likely because the AgNPs were added too late in the experiments. The effect of the TAgNPs were also troubled by the stabilizer, sodium citrate, as it gave the TAgNPs a negatively charged surface, creating electrostatic repulsion between the particles and the bacteria. This also made AFM measurements on a mica plate difficult. To better determine the bactericidal effect of SAgNPs, TAgNPs and silver ions, other techniques could have been used. One technique, is to determine the MIC and MLC on agar plates, giving a more quantifiable bactericidal effect. To further improve the bactericidal effect and understand how the surface-to-volume ratio affects the bactericidal effect of the AgNPs, another shape could be used like the tetrahedron with its large surface-to-volume ratio.

Bibliography

[1] Bakterierne bestemmer i vores krop. Illustreret Videnskab, 2003. Nr. 15.

[2] Keld Kjeldsen. *Infektionssygdomme og mikrobiologi*. Gyldendals Bogklubber, 2007.

[3] Kathleen Park Talaro. *Foundations in Microbiology*. McGraw-Hill, 2009.

[4] Gregor Reid and Jeremy Burton. Use of lactobacillus to prevent infection by pathogenic bacteria. *Microbes and Infection*, 4(3):319–324, 2002.

[5] RWK Wong, U Hagg, L Samaranayake, MKZ Yuen, CJ Seneviratne, and R Kao. Antimicrobial activity of chinese medicine herbs against common bacteria in oral biofilm. a pilot study. *International journal of oral and maxillofacial surgery*, 39(6):599–605, 2010.

[6] Fidel Martinez-Gutierrez, Peggy L. Olive, Adriana Banuelos, Erasmo Orrantia, Nereyda Nino, Elpidio Morales Sanchez, Facundo Ruiz, Horacio Bach, and Yossef Av-Gay. Synthesis, characterization, and evaluation of antimicrobial and cytotoxic effect of silver and titanium nanoparticles. *Nanomedicine: Nanotechnology, Biology, and Medicine*, 6:618–688, 2010.

[7] Mahendra Rai, Alka Yadav, and Aniket Gade. Silver nanoparticles as a new generation of antimicrobials. *Biotechnology Advances*, 27(1):76–83, 2009.

[8] Paulraj Kanmani and Seung Taik Lim. Synthesis and structural characterization of silver nanoparticles using bacterial exopolysaccharide and its antimicrobial activity against food and multidrug resistant pathogens. *Process Biochemistry*, 48:1099–1106, 2013.

[9] Sukumaran Prabhu and Eldho K. Poulose. Silver nanoparticles: mechanism of antimicrobial action, synthesis, medical applications, and toxicity effects. *International Nano Letters*, 2:1–10, 2012.

[10] Jun Sung Kim, Eunye Kuk, Kyeong Nam Yu, Jong-Ho Kim, Sung Jin Park, Hu Jang Lee, So Hyun Kim, Young Kyung Park, Yong Ho Park, Cheol-Yong Hwang, et al. Antimicrobial effects of silver nanoparticles. *Nanomedicine: Nanotechnology, Biology and Medicine*, 3(1):95–101, 2007.

[11] B. Ajitha and P. Ashok Kumar Reddy, Y. Sreedhara Reddy. Enhanced antimicrobial activity of silver nanoparticles with controlled particle size by ph variation. *Powder Technology*, 269:110–17, 2015.

[12] Melissa M Kemp, Ashavani Kumar, Dylan Clement, Pulickel Ajayan, Shaker Mousa, and Robert J Linhardt. Hyaluronan-and heparin-reduced silver nanoparticles with antimicrobial properties. *Nanomedicine*, 4(4):421–429, 2009.

[13] Jae Yong Song and Beom Soo Kim. Rapid biological synthesis of silver nanoparticles using plant leaf extracts. *Bioprocess and biosystems engineering*, 32(1):79–84, 2009.

[14] S Shiv Shankar, Akhilesh Rai, Absar Ahmad, and Murali Sastry. Rapid synthesis of au, ag, and bimetallic au core ag shell nanoparticles using neem (azadirachta indica) leaf broth. *Journal of colloid and interface science*, 275(2):496–502, 2004.

[15] Tanja Klaus, Ralph Joerger, Eva Olsson, and Claes-Göran Granqvist. Silver-based crystalline nanoparticles, microbially fabricated. *Proceedings of the National Academy of Sciences*, 96(24):13611–13614, 1999.

[16] Yasuhiro Konishi, Kaori Ohno, Norizoh Saitoh, Toshiyuki Nomura, Shinsuke Nagamine, Hajime Hishida, Yoshio Takahashi, and Tomoya Uruga. Bioreductive deposition of platinum nanoparticles on the bacterium shewanella algae. *Journal of biotechnology*, 128(3):648–653, 2007.

[17] Itamar Willner, Ronan Baron, and Bilha Willner. Growing metal nanoparticles by enzymes. *Advanced Materials*, 18(9):1109–1120, 2006.

[18] N Vigneshwaran, NM Ashtaputre, PV Varadarajan, RP Nachane, KM Paralikar, and RH Balasubramanya. Biological synthesis of silver nanoparticles using the fungus aspergillus flavus. *Materials letters*, 61(6):1413–1418, 2007.

[19] S Anil Kumar, Majid Kazemian Abyaneh, SW Gosavi, Sulabha K Kulkarni, Renu Pasricha, Absar Ahmad, and MI Khan. Nitrate reductase-mediated synthesis of silver nanoparticles from agno3. *Biotechnology Letters*, 29(3):439–445, 2007.

[20] R Geethalakshmi and Sarada DVL. Characterization and antimicrobial activity of gold and silver nanoparticles synthesized using saponin isolated from trianthema decandra l. *Industrial Crops and Products*, 51:107–115, 2013.

[21] Ahmad R Shahverdi, Sara Minaeian, Hamid Reza Shahverdi, Hossein Jamalifar, and Ashraf-Asadat Nohi. Rapid synthesis of silver nanoparticles using culture supernatants of enterobacteria: A novel biological approach. *Process Biochemistry*, 42(5):919–923, 2007.

[22] Ilana Perelshtein, Guy Applerot, Nina Perkas, Geoffrey Guibert, Serguei Mikhailov, and Aharon Gedanken. Sonochemical coating of silver nanoparticles on textile fabrics (nylon, polyester and cotton) and their antibacterial activity. *Nanotechnology*, 19(24):245705, 2008.

[23] Jin Zhou, Andrew L. Loftus, Geraldine Mulley, and A. Toby A. Jenkins. A thin film detection/response system for pathogenic bacteria. *Journal of the American Chemical Society*, 132(18):6566 – 6570, May 2010.

[24] Franck Furno, Kelly S Morley, Ben Wong, Barry L Sharp, Polly L Arnold, Steven M Howdle, Roger Bayston, Paul D Brown, Peter D Winship, and Helen J Reid. Silver nanoparticles and polymeric medical devices: a new approach to prevention of infection? *Journal of Antimicrobial Chemotherapy*, 54(6):1019–1024, 2004.

[25] Becton, Dickinson and Company (BD). *BD Bionutrients Technical Manual "Advanced Bioprocessing*, October 2006.

[26] American Type Culture Collection (ATCC). *ATCC BACTeriAl CulTure Guide "tips and techniques for culturing bacteria and bacteriophages"*, 2013.

[27] Alexander A Kokhanovsky. *Light Scattering Reviews 3: Light Scattering and Reflection*, volume 3. Springer, 2008.

[28] C Julian Chen. *Physics of solar energy*. John Wiley & Sons, 2011.

[29] Paw Dalgaard, Thomas Ross, Laura Kamperman, Karina Neumeyer, and Thomas A McMeekin. Estimation of bacterial growth rates from turbidimetric and viable count data. *International journal of food microbiology*, 23(3):391–404, 1994.

[30] James B. Kaper, James P. Nataro, and Harry L. T. Mobley. Pathogenic escherichia coii. *Nature Reviews Microbiology*, 2:123–140, 2004.

[31] Laura D Clements, Brian S Miller, and Uldis N Streips. Comparative growth analysis of the facultative anaerobes bacillus subtilis, bacillus licheniformis, and escherichia coli. *Systematic and applied microbiology*, 25(2):284–286, 2002.

[32] Peter Zuber. A peptide profile of the bacillus subtilis genome. *Peptides*, 22(10):1555–1577, 2001.

[33] L Korsten1 N Cook. Optimizing culturing conditions for bacillus subtilis.

[34] Maria Mercedes Palomino, Carmen Sanchez-Rivas, and Sandra M Ruzal. High salt stress in bacillus subtilis: involvement of pbp4 as a peptidoglycan hydrolase. *Research in microbiology*, 160(2):117–124, 2009.

[35] I Nicorescu, B Nguyen, M Moreau-Ferret, A Agoulon, S Chevalier, and N Orange. Pulsed light inactivation of bacillus subtilis vegetative cells in suspensions and spices. *Food Control*, 31(1):151–157, 2013.

[36] Bharat Bhushan, editor. *Springer Handbook of Nanotechnology*. Springer, 3rd edition, 2010.

[37] Anne Hansen, editor. *Nanoteknologiske Horisonter*. Danmarks Tekniske Universitet, 1st edition, 2010.

[38] C Ki. el. introduction to solid state physics, 2005.

[39] Paschalis Alexandridis and Marina Tsianou. Block copolymer-directed metal nanoparticle morphogenesis and organization. *European Polymer Journal*, 47(4):569–583, 2011.

[40] K Lance Kelly, Eduardo Coronado, Lin Lin Zhao, and George C Schatz. The optical properties of metal nanoparticles: the influence of size, shape, and dielectric environment. *The Journal of Physical Chemistry B*, 107(3):668–677, 2003.

[41] Michael Quinten. *Optical properties of nanoparticle systems: Mie and beyond*. John Wiley & Sons, 2010.

[42] Audrey Moores and Frederic Goettmann. The plasmon band in noble metal nanoparticles: an introduction to theory and applications. *New Journal of Chemistry*, 30:1121–1132, 2006.

[43] John R Reitz, Frederick J Milford, and Robert W Christy. *Foundations of electromagnetic theory*. Addison-Wesley Publishing Company, 2008.

[44] Peter B Johnson and R-W_ Christy. Optical constants of the noble metals. *Physical Review B*, 6(12):4370, 1972.

[45] JJ Mock, M Barbic, DR Smith, DA Schultz, and S Schultz. Shape effects in plasmon resonance of individual colloidal silver nanoparticles. *The Journal of Chemical Physics*, 116(15):6755–6759, 2002.

[46] Sihai Chen and David L Carroll. Synthesis and characterization of truncated triangular silver nanoplates. *Nano letters*, 2(9):1003–1007, 2002.

[47] Rongchao Jin, YunWei Cao, Chad A Mirkin, KL Kelly, George C Schatz, and JG Zheng. Photoinduced conversion of silver nanospheres to nanoprisms. *Science*, 294(5548):1901–1903, 2001.

[48] Lorraine Mulfinger, Sally D Solomon, Mozghan Bahadory, Aravindan V Jeyarajasingam, Susan A Rutkowsky, and Charles Boritz. Synthesis and study of silver nanoparticles. *Journal of Chemical Education*, 84(2):322, 2007.

[49] F. A. Cotton, G. Wilkinson, and P. L. Gaus. *Basic Inorganic Chemistry*. John Wiley & Sons, 1995.

[50] Dong Hua, Yang Hanxi, Ai Xinping, and Cha Chuansin. Hydrogen production from catalytic hydrolysis of sodium borohydride solution using nickel boride catalyst. *International Journal of Hydrogen Energy*, 28(10):1095–1100, 2003.

[51] Libor Kvitek, Aleš Panác ek, Jana Soukupova, Milan Kolar, Renata Vecerova, Robert Prucek, Mirka Holecová, and Radek Zboril. Effect of surfactants and polymers on stability and antibacterial activity of silver nanoparticles (nps). *The Journal of Physical Chemistry C*, 112(15):5825–5834, 2008.

[52] Thelma Serrano, Idalia Gómez, Rafael Colás, and José Cavazos. Synthesis of cds nanocrystals stabilized with sodium citrate. *Colloids and Surfaces A: Physicochemical and Engineering Aspects*, 338(1):20–24, 2009.

[53] Jill E Millstone, Sarah J Hurst, Gabriella S Métraux, Joshua I Cutler, and Chad A Mirkin. Colloidal gold and silver triangular nanoprisms. *Small*, 5(6):646–664, 2009.

[54] JM Kelly, GL Keegan, and ME Brennan-Fournet. Triangular silver nanoparticles: their preparation, functionalisation and properties. *Acta Physica Polonica-Series A General Physics*, 122(2):337, 2012.

[55] Catalina Marambio-Jones and Eric MV Hoek. A review of the antibacterial effects of silver nanomaterials and potential implications for human health and the environment. *Journal of Nanoparticle Research*, 12(5):1531–1551, 2010.

[56] Jose Ruben Morones, Jose Luis Elechiguerra, Alejandra Camacho, Katherine Holt, Juan B Kouri, Jose Tapia Ramírez, and Miguel Jose Yacaman. The bactericidal effect of silver nanoparticles. *Nanotechnology*, 16(10):2346, 2005.

[57] PV AshaRani, Grace Low Kah Mun, Manoor Prakash Hande, and Suresh Valiyaveettil. Cytotoxicity and genotoxicity of silver nanoparticles in human cells. *ACS nano*, 3(2):279–290, 2008.

[58] Jingyu Liu and Robert H Hurt. Ion release kinetics and particle persistence in aqueous nano-silver colloids. *Environmental science & technology*, 44(6):2169–2175, 2010.

[59] Zong-ming Xiu, Qing-bo Zhang, Hema L Puppala, Vicki L Colvin, and Pedro JJ Alvarez. Negligible particle-specific antibacterial activity of silver nanoparticles. *Nano letters*, 12(8):4271–4275, 2012.

[60] WJ Schreurs and H Rosenberg. Effect of silver ions on transport and retention of phosphate by escherichia coli. *Journal of bacteriology*, 152(1):7–13, 1982.

[61] PD Bragg and DJ Rainnie. The effect of silver ions on the respiratory chain of escherichia coli. *Canadian journal of microbiology*, 20(6):883–889, 1974.

[62] Katherine B Holt and Allen J Bard. Interaction of silver (i) ions with the respiratory chain of escherichia coli: an electrochemical and scanning electrochemical microscopy study of the antimicrobial mechanism of micromolar ag+. *Biochemistry*, 44(39):13214–13223, 2005.

[63] SY Liau, DC Read, WJ Pugh, JR Furr, and AD Russell. Interaction of silver nitrate with readily identifiable groups: relationship to the antibacterialaction of silver ions. *Letters in Applied Microbiology*, 25(4):279–283, 1997.

[64] Chun-Nam Lok, Chi-Ming Ho, Rong Chen, Qing-Yu He, Wing-Yiu Yu, Hongzhe Sun, Paul Kwong-Hang Tam, Jen-Fu Chiu, and Chi-Ming Che. Proteomic analysis of the mode of antibacterial action of silver nanoparticles. *Journal of Proteome research*, 5(4):916–924, 2006.

[65] QL Feng, Jian Wu, GQ Chen, FZ Cui, TN Kim, JO Kim, et al. A mechanistic study of the antibacterial effect of silver ions on escherichia coli and staphylococcus aureus. *Journal of biomedical materials research*, 52(4):662–668, 2000.

[66] Woo Kyung Jung, Hye Cheong Koo, Ki Woo Kim, Sook Shin, So Hyun Kim, and Yong Ho Park. Antibacterial activity and mechanism of action of the silver ion in staphylococcus aureus and escherichia coli. *Applied and environmental microbiology*, 74(7):2171–2178, 2008.

[67] H Arakawa, JF Neault, and HA Tajmir-Riahi. Silver (i) complexes with dna and rna studied by fourier transform infrared spectroscopy and capillary electrophoresis. *Biophysical journal*, 81(3):1580–1587, 2001.

[68] Okkyoung Choi, Kathy Kanjun Deng, Nam-Jung Kim, Louis Ross Jr, Rao Y Surampalli, and Zhiqiang Hu. The inhibitory effects of silver nanoparticles, silver

ions, and silver chloride colloids on microbial growth. *Water research*, 42(12):3066–3074, 2008.

[69] Hee-Jin Park, Jee Yeon Kim, Jaeeun Kim, Joon-Hee Lee, Ji-Sook Hahn, Man Bock Gu, and Jeyong Yoon. Silver-ion-mediated reactive oxygen species generation affecting bactericidal activity. *Water research*, 43(4):1027–1032, 2009.

[70] Andre Nel, Tian Xia, Lutz Mädler, and Ning Li. Toxic potential of materials at the nanolevel. *Science*, 311(5761):622–627, 2006.

[71] Eresha Mendis, Niranjan Rajapakse, Hee-Guk Byun, and Se-Kwon Kim. Investigation of jumbo squid (dosidicus gigas) skin gelatin peptides for their in vitro antioxidant effects. *Life Sciences*, 77(17):2166–2178, 2005.

[72] C Carlson, SM Hussain, AM Schrand, L K. Braydich-Stolle, KL Hess, RL Jones, and JJ Schlager. Unique cellular interaction of silver nanoparticles: size-dependent generation of reactive oxygen species. *The Journal of Physical Chemistry B*, 112(43):13608–13619, 2008.

[73] Gunnar Jansson and Mats Harms-Ringdahl. Stimulating effects of mercuric- and silver ions on the superoxide anion production in human polymorphonuclear leukocytes. *Free Radical Research*, 18(2):87–98, 1993.

[74] Ee Taek Hwang, Jin Hyung Lee, Yun Ju Chae, Yeon Seok Kim, Byoung Chan Kim, Byoung-In Sang, and Man Bock Gu. Analysis of the toxic mode of action of silver nanoparticles using stress-specific bioluminescent bacteria. *Small*, 4(6):746–750, 2008.

[75] M Raffi, F Hussain, TM Bhatti, JI Akhter, A Hameed, and MM Hasan. Antibacterial characterization of silver nanoparticles against e. coli atcc-15224. *Journal of Materials Science and Technology*, 24(2):192–196, 2008.

[76] Ivan Sondi and Branka Salopek-Sondi. Silver nanoparticles as antimicrobial agent: a case study on e. coli as a model for gram-negative bacteria. *Journal of colloid and interface science*, 275(1):177–182, 2004.

[77] Alexander B Smetana, Kenneth J Klabunde, George R Marchin, and Christopher M Sorensen. Biocidal activity of nanocrystalline silver powders and particles. *Langmuir*, 24(14):7457–7464, 2008.

[78] Siddhartha Shrivastava, Tanmay Bera, Arnab Roy, Gajendra Singh, P Ramachandrarao, and Debabrata Dash. Characterization of enhanced antibacterial effects of novel silver nanoparticles. *Nanotechnology*, 18(22):225103, 2007.

[79] Wen-Ru Li, Xiao-Bao Xie, Qing-Shan Shi, Hai-Yan Zeng, OU-Yang You-Sheng, and Yi-Ben Chen. Antibacterial activity and mechanism of silver nanoparticles on escherichia coli. *Applied microbiology and biotechnology*, 85(4):1115–1122, 2010.

[80] Nabil A Amro, Lakshmi P Kotra, Kapila Wadu-Mesthrige, Alexy Bulychev, Shahriar Mobashery, and Gang-yu Liu. High-resolution atomic force microscopy studies of the escherichia coli outer membrane: structural basis for permeability. *Langmuir*, 16(6):2789–2796, 2000.

[81] Sonit Kumar Gogoi, P Gopinath, Anumita Paul, A Ramesh, Siddhartha Sankar Ghosh, and Arun Chattopadhyay. Green fluorescent protein-expressing escherichia c oli as a model system for investigating the antimicrobial activities of silver nanoparticles. *Langmuir*, 22(22):9322–9328, 2006.

[82] Demberelnyamba Dorjnamjin, Maamaa Ariunaa, and Young Key Shim. Synthesis of silver nanoparticles using hydroxyl functionalized ionic liquids and their antimicrobial activity. *International journal of molecular sciences*, 9(5):807–820, 2008.

[83] Da-Guang Yu. Formation of colloidal silver nanoparticles stabilized by na< sup>+</sup>–poly (γ-glutamic acid)–silver nitrate complex via chemical reduction process. *Colloids and Surfaces B: Biointerfaces*, 59(2):171–178, 2007.

[84] Sukdeb Pal, Yu Kyung Tak, and Joon Myong Song. Does the antibacterial activity of silver nanoparticles depend on the shape of the nanoparticle? a study of the gram-negative bacterium escherichia coli. *Applied and environmental microbiology*, 73(6):1712–1720, 2007.

[85] Maribel Guzman, Jean Dille, and Stephane Godet. Synthesis and antibacterial activity of silver nanoparticles against gram-positive and gram-negative bacteria. *Nanomedicine: Nanotechnology, Biology and Medicine*, 8(1):37–45, 2012.

[86] Chang Hyun Bae, Sang Hwan Nam, and Seung Min Park. Formation of silver nanoparticles by laser ablation of a silver target in nacl solution. *Applied Surface Science*, 197:628–634, 2002.

[87] Prashant V Kamat, Mark Flumiani, and Gregory V Hartland. Picosecond dynamics of silver nanoclusters. photoejection of electrons and fragmentation. *The Journal of Physical Chemistry B*, 102(17):3123–3128, 1998.

[88] Binoj Nair and T Pradeep. Coalescence of nanoclusters and formation of submicron crystallites assisted by lactobacillus strains. *Crystal Growth & Design*, 2(4):293–298, 2002.

[89] Cristina Prieto and Lourdes Calvo. Performance of the biocompatible surfactant tween 80, for the formation of microemulsions suitable for new pharmaceutical processing. *Journal of Applied Chemistry*, 2013, 2013.

[90] Luis M Liz-Marzan, L. M.n and Isabel Lado-Tourino. Reduction and stabilization of silver nanoparticles in ethanol by nonionic surfactants. *Langmuir*, 12(15):3585–3589, 1996.

[91] Leif J Sherry, Rongchao Jin, Chad A Mirkin, George C Schatz, and Richard P Van Duyne. Localized surface plasmon resonance spectroscopy of single silver triangular nanoprisms. *Nano letters*, 6(9):2060–2065, 2006.

[92] MV Maslova, LG Gerasimova, and W Forsling. Surface properties of cleaved mica. *Colloid Journal*, 66(3):322–328, 2004.

[93] Isabel Pastoriza-Santos and Luis M Liz-Marzán. Synthesis of silver nanoprisms in dmf. *Nano Letters*, 2(8):903–905, 2002.

[94] Erika Soderstjerna, Patrik Bauer, Tommy Cedervall, Hodan Abdshill, Fredrik Johansson, and Ulrica Englund Johansson. Silver and gold nanoparticles exposure to in vitro cultured retina–studies on nanoparticle internalization, apoptosis, oxidative stress, glial-and microglial activity. *PloS one*, 9(8):e105359, 2014.

[95] Thawatchai Maneerung, Seiichi Tokura, and Ratana Rujiravanit. Impregnation of silver nanoparticles into bacterial cellulose for antimicrobial wound dressing. *Carbohydrate polymers*, 72(1):43–51, 2008.

[96] Anima Nanda and M Saravanan. Biosynthesis of silver nanoparticles from staphylococcus aureus and its antimicrobial activity against mrsa and mrse. *Nanomedicine: Nanotechnology, Biology and Medicine*, 5(4):452–456, 2009.

[97] Jayesh P Ruparelia, Arup Kumar Chatterjee, Siddhartha P Duttagupta, and Suparna Mukherji. Strain specificity in antimicrobial activity of silver and copper nanoparticles. *Acta Biomaterialia*, 4(3):707–716, 2008.

[98] Wen-Ru Li, Xiao-Bao Xie, Qing-Shan Shi, Shun-Shan Duan, You-Sheng Ouyang, and Yi-Ben Chen. Antibacterial effect of silver nanoparticles on staphylococcus aureus. *Biometals*, 24(1):135–141, 2011.

[99] Ales Panacek, Libor Kvitek, Robert Prucek, Milan Kolar, Renata Vecerova, Nadezda Pizurova, Virender K Sharma, Tat'jana Nevec na, and Radek Zboril. Silver colloid nanoparticles: synthesis, characterization, and their antibacterial activity. *The Journal of Physical Chemistry B*, 110(33):16248–16253, 2006.

[100] Benjamin Wiley, Thurston Herricks, Yugang Sun, and Younan Xia. Polyol synthesis of silver nanoparticles: use of chloride and oxygen to promote the formation of single-crystal, truncated cubes and tetrahedrons. *Nano Letters*, 4(9):1733–1739, 2004.

[101] TJ Beveridge and RG Murray. Sites of metal deposition in the cell wall of bacillus subtilis. *Journal of Bacteriology*, 141(2):876–887, 1980.